

Single-crystal dating and the detrital record of orogenesis

DOUGLAS W. BURBANK*, IAN D. BREWER†, EDWARD R. SOBEL‡
and MICHAEL E. BULLEN†

*Department of Earth Science, University of California, Santa Barbara, CA 93106, USA (Email: burbank@crustal.ucsb.edu)

†Department of Geosciences, Pennsylvania State University, University Park, PA 16802, USA

‡Institut fuer Geowissenschaften, Universitaet Potsdam, Postfach 601553, 14415 Potsdam, Germany

ABSTRACT

Single-crystal dating of detrital mineral grains confers a remarkable ability to reconstruct cooling histories of orogens and to place limits on the timing, magnitude, and spatial variations of erosion. Numerous grains from a detrital sample are typically dated, and the statistical variability between populations of ages in different samples provides keys to variations in cooling histories and exhumation rates within the hinterland. Given that detrital samples comprise minerals drawn from an entire catchment, they offer an integrated perspective that is almost always unattainable with bedrock samples. Moreover, because detrital ages are preserved within stratigraphic successions, the evolution of populations of cooling ages through time and across an orogen can be reconstructed from the sedimentary record. When combined with a known hinterland 'stratigraphy' of bedrock cooling ages, studies of detrital ages in modern river systems demonstrate the fidelity of the detrital signal, and reveal both the power and limitations of detrital single-crystal dating in sedimentary basins. Low-temperature thermochronometers can be sensitive to variations in hinterland erosion of as little as 1–2 km. Although recognized previously from a theoretical viewpoint, the impact exerted on modern detrital ages by the interplay between erosion rates and lithology within tributary catchments has only recently been documented and provides a basis for refining orogenic histories using detrital ages. Documentation of the downstream evolution of detrital ages emphasizes that the distribution of ages that reaches the mouth of a river may bear little resemblance to age distributions in the headwaters. Similarly, because lithological concentrations of minerals used for single-crystal dating can vary by many fold within the hinterland, rapidly eroding tributary catchments do not necessarily dominate populations of detrital ages. An ability to exploit detrital ages to place limits on kinematic rates within collisional orogens as a function of cooling rates provides a potent new analytical tool. If uncertainties regarding kinematic geometries, related particle pathways through orogens and steady-state assumptions can be reduced, detrital ages in both modern rivers and the recent stratigraphical record can serve to reconstruct rates of deformation and erosion and to test the viability of proposed models of orogenic evolution.

Keywords Detrital ages, single-crystal dating, methodologies, erosion rates, controls on detrital record, Himalaya, Tien Shan.

INTRODUCTION

Cooling histories of orogens represent responses to tectonic denudation, such as extensional faulting (Davis, 1988), and to erosion by geomorphological processes. As erosion removes rock at the Earth's surface, rock at depth moves toward the surface and

cools. As individual minerals in these rocks cool below their radiometric 'closure' temperature and retain the products of radiometric decay, they begin to record the time since cooling below that critical temperature. Minerals with high closure temperatures may not be affected by cooling events that affect minerals with sensitivity to lower temperatures. For

example, U–Pb ages on zircons commonly represent crystallization ages of rocks, whereas $^{39}\text{Ar}/^{40}\text{Ar}$ ages on hornblende or muscovite and fission-track ages on zircon record cooling of a rock below $\sim 525^\circ\text{C}$, 350°C and $\sim 250^\circ\text{C}$, respectively (McDougall & Harrison, 1988; Yamada *et al.*, 1995).

It can be difficult to determine whether extensional faulting, waning magmatic processes, or geomorphic erosion has caused the cooling recorded by various thermochronometers. Cooling of minerals through higher temperatures ($300\text{--}600^\circ\text{C}$) typically occurs at depths > 10 km, so field evidence of extensional faulting may be removed during subsequent erosion. Consequently, the driving mechanism for cooling may remain ambiguous. For minerals with lower closure temperatures ($< 150^\circ\text{C}$), however, geological evidence for extensional faulting, if it has occurred, is likely to be preserved. For low-temperature thermochronology, therefore, absence of evidence for extensional faulting indicates that cooling is primarily or entirely due to erosion by surface processes.

Irrespective of the crustal depth at which thermochronologically relevant cooling occurs, upon reaching the surface, the sediment derived from these rocks typically retains the age information about when they cooled through their respective closure temperatures. Hence, the distribution of cooling ages in detrital sediment contains a record of the cooling history of the rocks from which the sediment was eroded (Garver & Brandon, 1994).

The advent of single-crystal dating has allowed precise determination of individual cooling ages. Initial success in the 1980s utilized fission-track dating of detrital zircon (Cerveny *et al.*, 1988), but now single-crystal dating is routinely done with $^{39}\text{Ar}/^{40}\text{Ar}$, U–Pb, and other methods (Gehrels & Kapp, 1998; Brewer *et al.*, 2003; Wobus *et al.*, 2003; Ruhl & Hodges, 2005). Thus, it is now possible to examine hundreds of individual grain ages from a sediment sample, either modern or ancient. It is even possible (though rarely done) to date minerals from the same sample with different methods, such as by combining fission-track with U–Pb ages (Carter & Moss, 1999; Reiners *et al.*, 2004).

Single-crystal dating provides a new perspective on reconstructing the cooling/erosional history of an orogen. Two specific applications have become common. Samples collected sequentially within a stratigraphic section can be analysed to yield a

step-by-step reconstruction of changes in the suite of mineral cooling ages emerging from an orogen (e.g. Carter & Moss, 1999; White *et al.*, 2002; Reiners *et al.*, 2004). Analysis of detrital sediments in modern streams yields a broad sampling of the realm of cooling ages presently exposed within a tributary catchment (e.g. Bernet *et al.*, 2004a). As opposed to the single cooling age typically derived from an individual bedrock sample, detrital ages display an unparalleled attribute: they represent a collection of bedrock cooling ages from throughout a catchment. As such, detrital samples can provide a potent synthesis of information on catchment-wide cooling ages.

Occasionally, the stratigraphic and modern-stream approaches have been combined. For example, one of the first single-crystal age studies (Cerveny *et al.*, 1988) looked at the age distributions of detrital zircon both in the modern Indus River in Pakistan, as well as in Indus foreland strata that dated back to ~ 14 Ma (Fig. 1a). This study identified very young detrital ages (~ 1 Ma) in the modern river and concluded that, because these ages indicated cooling rates of $\sim 200^\circ\text{C Myr}^{-1}$, they represented very rapid erosion (≥ 3 mm yr^{-1}) somewhere in the hinterland. Moreover, within the stratigraphic sequence, when the depositional ages and the cooling ages were compared, Cerveny *et al.* (1988) showed that zircons with similarly young cooling ages (1–2 Myr) had been deposited in the foreland throughout the past 14 Myr (Fig. 1b). The only known modern source for cooling ages this young was the Nanga Parbat–Haramosh massif (Zeitler, 1985), and Cerveny *et al.* (1988) reached the important conclusion that uplifts similar to Nanga Parbat must have persisted in the northwestern Himalaya since at least middle Miocene times. This pioneering study demonstrated the potential of detrital ages to reveal a time series of cooling histories and of reconstructed erosion rates that had previously been inaccessible.

The present study focuses on concepts related to detrital mineral ages, on tests of the assumptions that underpin interpretations of cooling ages, and on some new applications of detrital cooling ages to tectonic problems. After reviewing how bedrock and sedimentary cooling ages are generated and common ways of interpreting detrital age data, we ask:

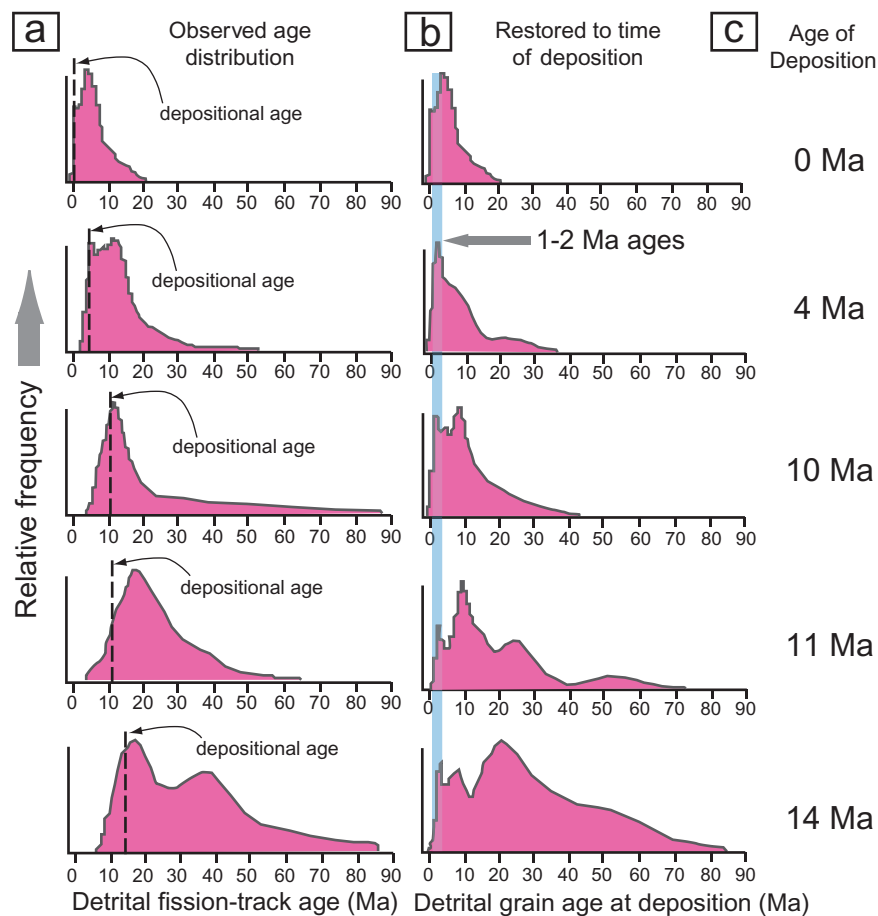


Fig. 1 Single-crystal fission-track age populations of detrital zircons in the northwest Himalaya (modified from Cervený *et al.*, 1988). (a) Observed ages in the modern Indus River (0 Ma) and at stratigraphic horizons of known age extending back to 14 Ma. The stratigraphic levels were dated using magnetostratigraphy (Johnson *et al.*, 1985) and have uncertainties of ~ 0.5 Myr. Note that for all sites other than the modern site, some fission-track ages are younger than the time of deposition. These samples have never been heated sufficiently to anneal fission tracks following deposition (which reset the ages), so these 'too-young' ages are likely to result from the statistics of counting small numbers of spontaneous fission tracks, and due to the relatively large uncertainties (typically $\sim 10\%$) that characterize fission-track dating. (b) Detrital ages restored back to the time of deposition. Restoration is accomplished both by subtracting the depositional age from each detrital age (c) and through accounting for the statistical uncertainties inherent in populations of fission-track dates (see Cervený *et al.* (1988) for a more thorough description). Notably, young (1–2 Myr) ages are present in each of the restored population of ages. These young ages require cooling at rates of $> 100^\circ\text{C Myr}^{-1}$, and they indicate that rapid erosion was occurring somewhere in the Indus catchment throughout the past 14 Myr.

1 To what extent do cooling ages in sediments match model predictions of age distributions and frequencies?

2 How does the detrital cooling-age signal evolve as it passes through an orogen from headwater regions to an adjacent basin?

3 To what extent do hinterland variations in lithology or erosion rates control the contributions of cooling ages from each tributary?

4 How can distributions of detrital mineral ages be used to place viable constraints on tectonic rates?

Through comparison of observed bedrock cooling ages in the northern Tien Shan with nearby ancient and modern sediments, it is shown that: (i) modern detrital ages are matched by a combination of a known bedrock age stratigraphy, basin relief and basin hypsometry; and (ii) along-strike differences in modern detrital age distributions correlate with changes in the timing and magnitude of uplift and dissection of the range. By tracking cooling-age distributions in modern sediment along

a river that traverses the Himalaya of central Nepal, we explore how variations in rates of bedrock erosion, lithology and basin size are convolved to create the trunk-stream detrital age signal. Finally, cooling ages in a collisional orogen are predicted using a simple thermo-mechanical model and then the observed detrital cooling ages are used to place limits on the rates of deformation within the orogen.

CONCEPTS OF BEDROCK COOLING AGES

All minerals used in thermochronological studies have critical temperatures at which they begin to record time. In reality, this critical temperature is a range of values that can be compositionally dependent, but conceptually this temperature can be considered as a discrete value: the 'closure' temperature (Dodson, 1979). For most radiometric approaches, such as the $^{39}\text{Ar}/^{40}\text{Ar}$ or U–Pb systems, the ratio of parent radiometric nuclides to their daughter products is used to define a cooling age. At temperatures higher than the closure temperature, radiometric daughter products are lost by rapid diffusion through the crystal lattice. Once cooled below the closure temperature, the mineral lattice retains the daughter nuclides and the radiometric clock starts.

In fission-track dating, rather than producing daughter nuclides that are subsequently measured, fissioning of uranium creates fragments that tear in opposite directions through the mineral lattice for $\sim 8\ \mu\text{m}$ in each direction in apatites and $\sim 5.5\ \text{mm}$ in zircon (Carter, 1999). At high temperatures, the lattice gradually restores its original geometry and anneals the damage zone. At temperatures less than the 'annealing' temperature, repair of the lattice damage is sufficiently slow that fission tracks are preserved. The two minerals apatite and zircon, most commonly used in fission-track dating, have nominal closure temperatures (below which tracks are preserved) of 110°C and $\sim 250^\circ\text{C}$, respectively (Naeser, 1979; Yamada *et al.*, 1995). The closure temperature is sensitive to the rate of cooling, such that apatite crystals that cool at $> 100^\circ\text{C}\ \text{Myr}^{-1}$ have closure temperatures of $\sim 140^\circ\text{C}$ (Dodson, 1979). The closure temperature is also sensitive to composition: chlorapatites have closure temperatures that are as much as $\sim 50^\circ\text{C}$ higher than the

more commonly occurring fluorapatites (Ketcham *et al.*, 1999).

Annealing does not stop abruptly at a given temperature, so a 'partial annealing zone' (PAZ) exists between the nominal closure temperature and temperatures $< 60^\circ\text{C}$ at which fission tracks become essentially permanent. Thus, a structure of ages is predicted to exist in the subsurface (Fig. 2). The trends of ages in the rock above the PAZ should reflect the previously cooling history. If these ages show little variation with depth, they indicate that this part of the rock column cooled rapidly during the penultimate episode of erosion and uplift, whereas a steady and large downward decrease in ages would indicate a sustained interval of slow erosion. For typical geothermal gradients, the PAZ is 2–3 km thick. At its top (Fig. 2a), a downward trajectory of decreasing ages begins. The rate of decrease of ages with depth in the PAZ depends on the time since the last major cooling episode (compare Fig. 2a & b): the rate increases with greater elapsed time since the penultimate cooling event. The base of the PAZ is marked by a 'kink' below which all ages are zero, because temperatures greater or equal to the closure temperature have been encountered. If this column of rock is suddenly subjected to rapid rock uplift and erosion in response to tectonic events, the former PAZ will be raised toward the surface (Fig. 2c), and the kink formerly at its base should be preserved during uplift (Fitzgerald *et al.*, 1995). If the amount of erosion exceeds 4–5 km, then the rocks at the base of the former PAZ are likely to be exposed at the surface. The ages just below the kink are commonly interpreted to indicate the time that accelerated erosion began (Fig. 2c), whereas the thickness of the zone of nearly uniform ages beneath the kink provides a minimum limit on the amount of erosion during that event.

For a particular mineral, the cooling ages observed at the surface of a mountain belt are a function of the rate of erosion and the depth of the relevant closure isotherm. Most commonly, cooling ages have been interpreted using a geothermal gradient that is assumed to be both vertically and spatially uniform (Zeitler, 1985; Tippett & Kamp, 1993; Fitzgerald *et al.*, 1995; Blythe *et al.*, 2002). In this case, the depth of a given isotherm will be everywhere the same beneath the mean surface elevation. By applying a known or assumed geothermal

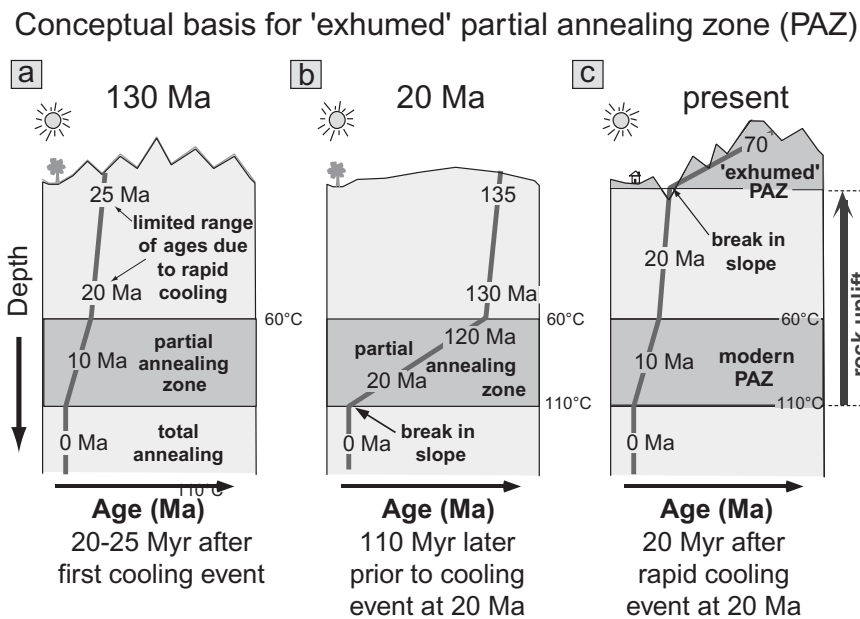


Fig. 2 Patterns of fission-track ages and the partial annealing zone (PAZ) versus depth at different times that span an interval of rapid erosion. (a) Predicted pattern of ages at 130 Ma, which illustrates conditions 20 Myr after a still-earlier major cooling event. Rapid cooling and extensive erosion could be interpreted for that event because the ages above the PAZ are very similar, such that only a small change in age versus depth occurs. Note that ages within the PAZ gradually decrease to 0 at its base where temperatures $> 110^{\circ}\text{C}$ are first encountered. (b) Pattern of ages at 20 Ma following a long interval (110 Myr) of quiescence. Note the greatly increased range of ages within the PAZ compared with (a). (c) Ages at present. The former PAZ (now 'exhumed') has been raised to the surface. The ages at the kink at the base of the PAZ indicate the time (20 Ma) of the uplift/erosion event. Note that the gradient of ages in the PAZ is now identical to that in the first panel which also depicts a time 20 Myr after a major uplift/erosion event.

gradient to define that depth (z), cooling ages (t) can be readily converted into erosion rates (dz/dt).

Such an analysis is a simplification of the more typical situation in a mountain range, in which ridges act like radiator fins and affect the pattern of cooling and position of isotherms in the subsurface (Stüwe *et al.*, 1994; Mancktelow & Grasemann, 1997; Stüwe & Hintermüller, 2000). Isotherms are warped upward beneath ridges and are more widely spaced than they are beneath valleys. The amount of warping is a function of the topographic relief and the rate of erosion (Fig. 3). This compression of isotherms toward the surface and especially beneath valleys can be understood in the context of rock that is advected toward the erosional surface: rapid erosion causes rapid advection which in turn causes hotter rocks from depth to be brought more quickly toward the surface, thereby increasing the near-surface geothermal gradient. The greater the topographic relief, the more that isotherms are deflected upward beneath the ridges.

The greater the erosion rate, the greater the compression of the isotherms beneath the valleys.

One key conclusion from analyses of isotherms in the context of variable topographic relief and erosion rates is that, at any point in the landscape, the geothermal gradient is not uniform (Stüwe *et al.*, 1994; Mancktelow & Grasemann, 1997; Stüwe & Hintermüller, 2000). As well as having higher gradients under valleys than beneath ridges and higher gradients when erosion is rapid, the gradient is also higher near the surface than at depth (Fig. 3). As a consequence, application of an assumed uniform geothermal gradient is compromised, especially for minerals with low closure temperatures and in regions of rapid erosion and high relief. Thus, the effects of topography are particularly significant for fission-track or [U-Th]/He dating of apatite with their sensitivity to the 110°C and 70°C isotherms, respectively. For minerals with higher closure temperatures, the assumption of a uniform geotherm is less problematic. For

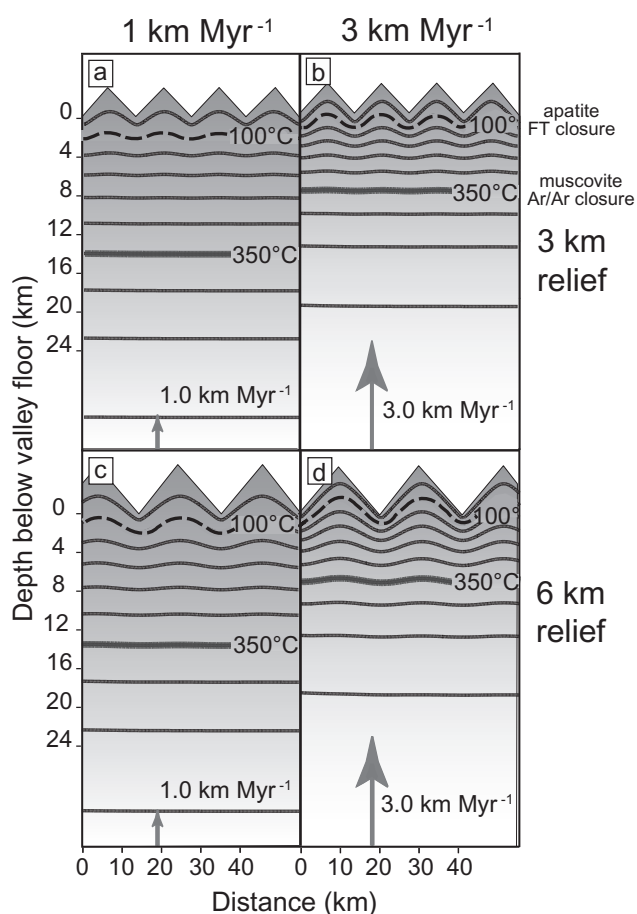


Fig. 3 Numerical modelling prediction of thermal structure of continental crust, given specified erosion rate, topographic relief and wavelength, and hillslope angle. The thermal structure is equivalent to a thermal steady state and occurs before 20 Myr in model runs. Relief production is instantaneous at the start of the model run, with a steady-state landscape that contains 30° slopes, which simulate threshold conditions for landsliding. The depth and deflection of individual isotherms depend on topographic relief and the rate of erosion, with the lower temperature isotherms being most affected. High relief and rapid erosion rates cause the maximum amount of deflection of the isotherms beneath the peaks, as well as the maximum compression of isotherms beneath valleys. (a & b) Erosion rates of 1.0 km Myr⁻¹ and 3.0 km Myr⁻¹ are imposed on a landscape with 3 km of relief. (c & d) Relief is increased to 6 km with the same erosion rates. Note that the 350°C closure isotherm for ⁴⁰Ar/³⁹Ar in muscovite is predicted to be essentially flat, except when erosion is ≥ 3 km Myr⁻¹ and topographic relief is ≥ 6 km, in which case the depth of the 350°C isotherm varies by ~ 200 m. (Modified from Brewer, 2001.)

example, for muscovite that is dated using ³⁹Ar/⁴⁰Ar techniques, the relevant closure temperature is ~ 350°C. As long as topographic relief remains < 6 km and erosion rates are ≤ 3 mm yr⁻¹, numerical modelling suggests that the 350°C isotherm remains nearly horizontal beneath the mean topography (Brewer *et al.*, 2003), although this isotherm will have been advected closer to the surface when erosion rates are high (Fig. 3).

In addition to topographic controls on isotherms, faulting can also have important thermal effects (Ehlers & Farley, 2003; Bollinger *et al.*, 2004; Jamieson *et al.*, 2004). Underthrusting of colder rock beneath a hangingwall refrigerates the hangingwall and perturbs the thermal structure. In extensional settings, tilting of the footwall during faulting will reorient isotherms (Ehlers *et al.*, 2003). The net result of faulting in active orogens is that cooling ages become less directly linked to the rate of vertical erosion at any particular site on the surface. Additional variability in isotherms results from spatial differences in radioactive heat production and from variations in subsurface fluid flow and thermal conductivity, which promote heat advection that can be largely independent of the rate of rock advection.

CONCEPTS OF DETRITAL COOLING AGES

Sediments eroded from orogens are commonly preserved in the foreland basin or in large delta complexes of major river systems (e.g. the Indus or Bengal fans). Detrital cooling ages extracted from such sediment should be a representation of cooling ages within the river's catchment (Stock & Montgomery, 1996; Bernet *et al.*, 2004b). The ways in which this signal is produced can be more readily conceptualized if it is considered how tributary areas of the main river contribute cooling ages to the trunk river as it flows from the hinterland to the site of deposition. It is helpful to target tributary areas at spatial scales for which erosion and cooling rates within a catchment are nearly uniform.

Given a prediction of bedrock cooling ages in a tributary catchment, conceptualization of how the detrital age signal should develop within an orogen is straightforward (Stock & Montgomery, 1996). Every tributary to a trunk stream should

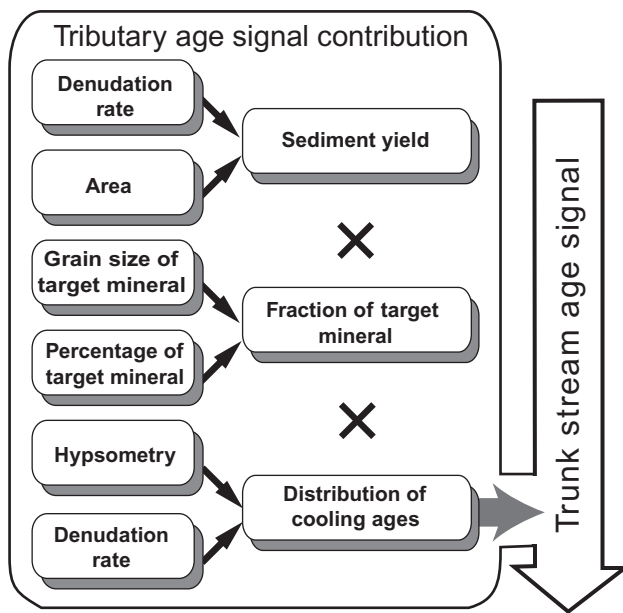


Fig. 4 Parameters controlling the contribution of cooling ages from an individual tributary to a trunk-stream cooling-age signal. Either the trunk-stream or the foreland-basin signal can be modelled as a specified mix of several such tributaries. The tributary area and the average denudation rate define the total sediment yield. The abundance of the mineral to be dated and the size distribution of the target mineral determine the fraction of grains in the total sample that could be dated. The denudation rate (assumed to have persisted long enough to create steady-state thermal conditions) and the hypsometry combine to determine the range and abundance of cooling ages. The product of the total sediment yield, the fraction of the target mineral and the frequency distribution of cooling ages define the tributary's contribution to the distribution of individual grain ages in the trunk stream.

contribute a sediment volume proportional to its catchment area and the average erosion rate within it (Fig. 4). If erosion has persisted sufficiently long to achieve a thermal steady state (Willett & Brandon, 2002), the range of cooling ages should be a predictable function of the basin relief and erosion rate (Fig. 5a). If the distribution of the mineral that is targeted for dating is uniform within the catchment, the distribution of cooling ages (Fig. 5b) will be a direct function of the erosion rates and catchment hypsometry (the distribution of area versus altitude; Brewer *et al.*, 2003). Finally, to calculate how a tributary's flux of cooling ages

will affect the cooling-age distribution of the trunk stream, the fraction of the target mineral, including its abundance in the size fraction being dated, must be compared between the tributary sediment and that of the trunk stream (Fig. 4). If the target mineral for dating is in low abundance, e.g. zircon in limestone, then even a large and rapidly eroding catchment will have a minimal impact on the cooling ages in the trunk stream (Spiegel *et al.*, 2004). Within this conceptual framework, it is possible to work progressively downstream and model how the trunk stream signal will evolve with the addition of material from tributaries with varying characteristics.

The direct prediction of the distribution of detrital ages (Fig. 5) that results from combining an erosion rate and a catchment hypsometry (Brewer *et al.*, 2003) means that observed detrital age distributions can, in theory, be used to infer combinations of hypsometry and erosion rates within the tributary catchment. For example, if a hypsometry with topography distributed as a simple Gaussian function is assumed, then straightforward predictions of the effects of changes in erosion rates and relief can be made (Fig. 6). As erosion rates increase, the mean of the detrital ages becomes increasingly young. As relief increases, the breadth of detrital ages increases, due to the age difference between valley bottoms and ridge crests (Figs 5 & 6). Such changes provide a theoretical basis for using cooling-age distributions to test hypotheses, such as those related to increased relief production (Small & Anderson, 1998) and/or enhanced erosion rates during Late Cenozoic times (Zhang *et al.*, 2001). Successful testing with this approach, however, requires high-resolution dating and a stratigraphic section in a basin that has had a stable tributary catchment over the period of interest. Recent experimental and numerical studies, however, suggest that drainage divides will migrate over time (Hasbargen & Paola, 2000, 2002; Pelletier, 2004), and relative changes in catchment location and geology due to divide migration must be small relative to overall catchment size for the catchment to be considered stable. Without an extensive knowledge of the evolution of the hinterland that permits fingerprinting of distinct source areas (Spiegel *et al.*, 2004), assessment of the dominance and persistence of source areas is rarely possible.

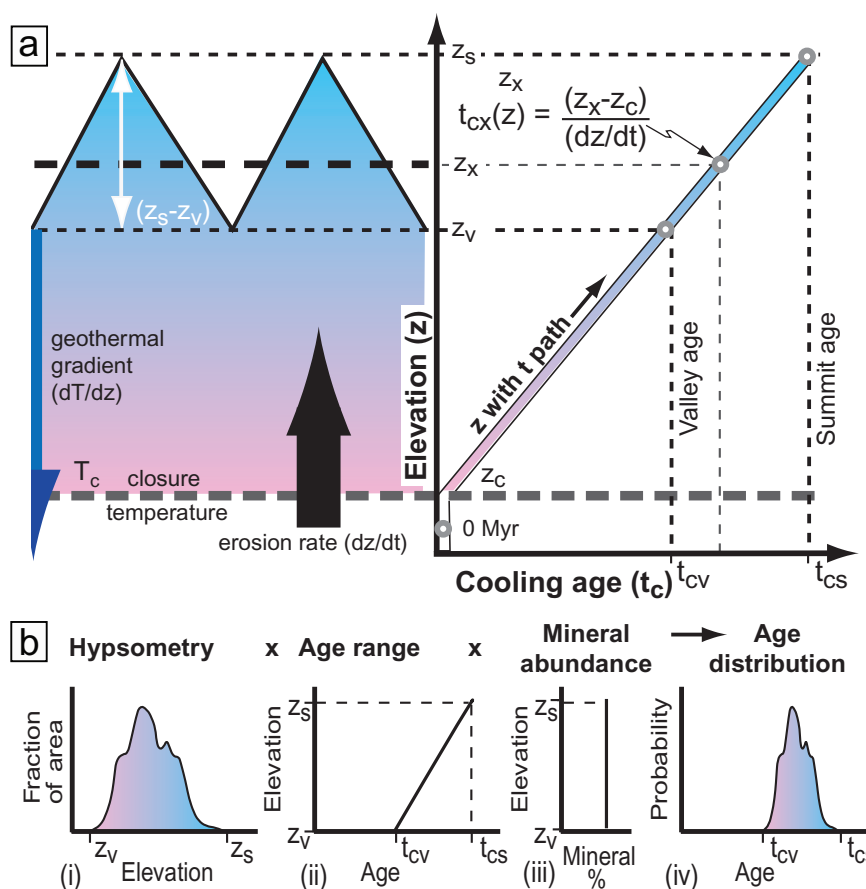


Fig. 5 Construction of a 'theoretical' distribution of bedrock cooling ages for an individual catchment. (a) A cooling age (t_c) is calculated from the depth (z_c) of the closure temperature (T_c) for which z_c results from a thermal model and the erosion rate (dz/dt). The difference between summit elevation (z_s) and valley elevation (z_v) creates a difference between summit cooling ages (t_{cs}) and the valley cooling ages (t_{cv}). The cooling age (t_{cx}) of a sample 'x' derived from elevation z_x can be calculated using the equation shown. (b) The frequency distribution of cooling ages is governed by the combination of the age range (t_{cv} to t_{cs}) and the altitude-dependent frequency of the target mineral (here assumed to be uniform) with the hypsometry of the catchment. The direct correspondence of the hypsometry and the distribution of cooling ages results from the uniform distribution of the target mineral throughout the catchment. (Modified from Brewer *et al.*, 2003.)

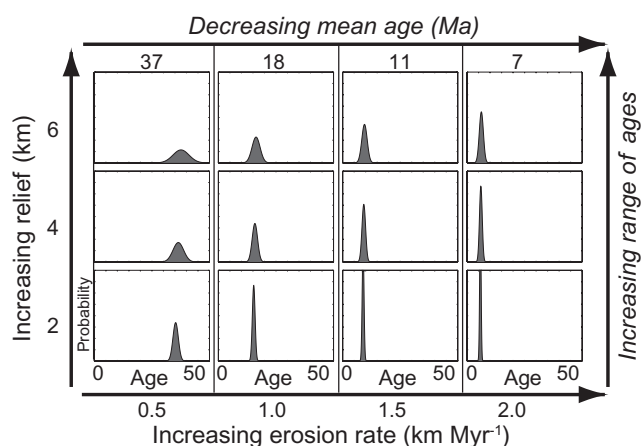


Fig. 6 (left) Theoretical effects of variations in uplift rate and relief on cooling-age distributions for a source-area catchment with a Gaussian-distributed hypsometry. The depth to the 350°C isotherm is modelled as a function of erosion rate and topographic relief (Stüwe *et al.*, 1994). The scale of each inset theoretical probability density function plot is the same, with the x axis ranging from 0 to 50 Myr and probability on the y axis. The area under the curve in each plot is normalized to one. According to these models, changes in relief or erosion rate should be manifested by changes in the central age and the spread of ages found within a catchment. For any given relief, slower erosion rates produce a broader range of cooling ages. Similarly, for a given erosion rate, greater relief yields a broader range of ages. (Modified from Brewer *et al.*, 2003.)

Thus, although changes in the range and distribution of cooling ages are predictable based on variations in relief and erosion rate (Fig. 6), these concepts can be practically applied only in unusual circumstances in which the source area can be shown to be stable through time.

OROGENIC EVOLUTION, LAG TIMES AND APPLICATIONS OF DETRITAL AGES

The preceding discussion indicates that, prior to an interval of accelerated rock uplift and erosion, a 'stratigraphy' of cooling ages for low-temperature

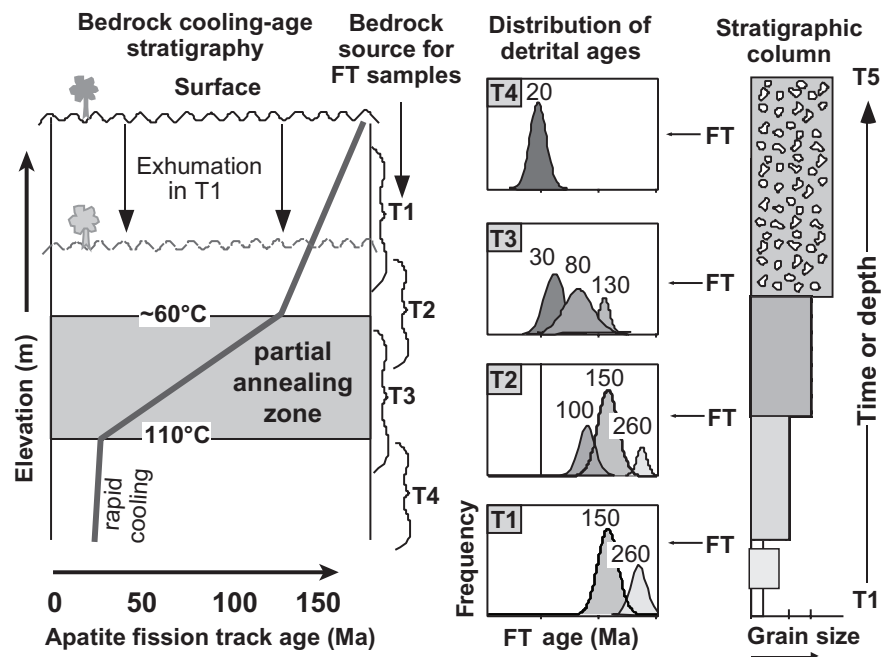


Fig. 7 Model for detrital mineral populations resulting from progressive unroofing (at times T1 to T4) through a crustal column that preserves an exhumed apatite partial annealing zone (PAZ) in which ages span from 25 to 125 Ma. Apatite is assumed to be uniformly distributed in the crustal column. The stratigraphic column on the right depicts a coarsening upward sequence in which 'FT' indicates the stratigraphic level at which four detrital fission-track samples are analysed. The primary component age distributions (Brandon, 1992) are illustrated for each detrital sample (centre column) with the central age of each component shown in 'million years ago'. Progressive erosion of a crustal column with a given age–elevation succession is predicted to produce an inverse age stratigraphy in an adjacent basin. Time-step T1 represents erosion only through the region of older cooling ages that sits above the PAZ in the crustal column. Consequently, the detrital age distribution contains only older age populations. For successively higher and younger stratigraphic levels, erosion in the hinterland has progressed down into the (now exhumed) PAZ. The youngest component age-peak reflects the deepest level of erosion at any given time. When Tertiary ages first appear (stage T3), erosion has progressed deeply into the PAZ. For the youngest sample (T4), only reset samples with Tertiary ages are predicted, suggesting erosion entirely through the PAZ.

thermochronometers commonly exists within a vertical column of slowly eroding bedrock (Stock & Montgomery, 1996). The youngest ages (0 Ma) occur at depths where the temperature exceeds the closure temperature, while the oldest ages occur near the surface, where they reflect previous thermal events (Fig. 2). Accelerated erosion that slices progressively deeper through this rock column would be expected to yield an inverted age stratigraphy in an adjacent basin (Fig. 7). Consequently, detrital ages from a stratigraphic section should be expected to record the progressive unroofing of the hinterland (Brown, 1991; Gallagher *et al.*, 1998; Carter & Moss, 1999). Most significantly, in the context of fission-track dating, the beginning of unroofing of the partial annealing zone (PAZ) should

be clearly evidenced by the abrupt appearance of younger detrital ages. Such an event indicates that erosion in the hinterland has proceeded significantly below a depth that was formerly at ~60°C (top of the PAZ: Fig. 2), typically at 2–3 km initial depth. As detrital ages more closely approach the depositional age, it is likely that the rocks previously situated beneath the PAZ (at depths exceeding 3.5–5 km) are now being eroded. Under these conditions and assuming the occurrence of apatite is approximately uniform in the source area, the detrital record within a well-dated basin stratigraphy provides detailed insights on the progressive erosion of the hinterland (Fig. 7).

The 'lag time' is defined as the time it takes for a mineral to pass from its closure temperature at

some depth below the surface to its deposition in a sedimentary basin (Cerveny *et al.*, 1988; Garver & Brandon, 1994). In a mountain belt, this lag time encompasses two suites of processes: those responsible for bringing the mineral to the surface from some depth-dependent temperature; and those responsible for transporting the mineral from the orogen to a sedimentary basin (Ruiz *et al.*, 2004). In many active orogens, the transport time from when the mineral first reaches the surface to when it is deposited in a basin is considered to be negligible. In rapidly eroding mountains ($> 0.5 \text{ mm yr}^{-1}$), such an assumption can be broadly validated simply by comparing volumes of stored sediments, or of potential storage within the mountain catchments, with the amount of sediment produced by persistent erosion. Typically, only a tiny fraction of the overall volume of sediments eroded could be stored for more than a few hundred thousand years. If the transport time can be argued to be negligible, then the lag time represents the time required for a mineral to pass from the closure isotherm to the surface and becomes a proxy for the rate of erosion. Therefore, for the record of unroofing in a nearby basin, the lag time represents the difference between the cooling age and the depositional age. As the detrital age approaches progressively closer to the depositional age, i.e. lag times shorten, the reconstructed rate of cooling of the source area becomes increasingly rapid, as does the correlative rate of hinterland erosion.

Given this framework, lag times can be used to assess the erosional state of an orogen (Fig. 8). Much current debate revolves around the question of whether orogens can attain a steady-state condition (Willett & Brandon, 2002), and if they do so, how rapidly and by what processes does this occur. For example, orogenic steady state has been defined in terms of exhumational steady state (in which cooling ages at a given position in the orogen remain constant through time) or thermal steady state (in which the thermal structure with respect to the surface is invariant; Willett & Brandon, 2002). In either case, the overall distribution of cooling ages at the surface of a steady-state orogen is predicted to remain constant through time. If the sediment transport time is either negligible or predictable, such that it can be subtracted from the cooling age, then a steady-state orogen should yield consistent lag times.

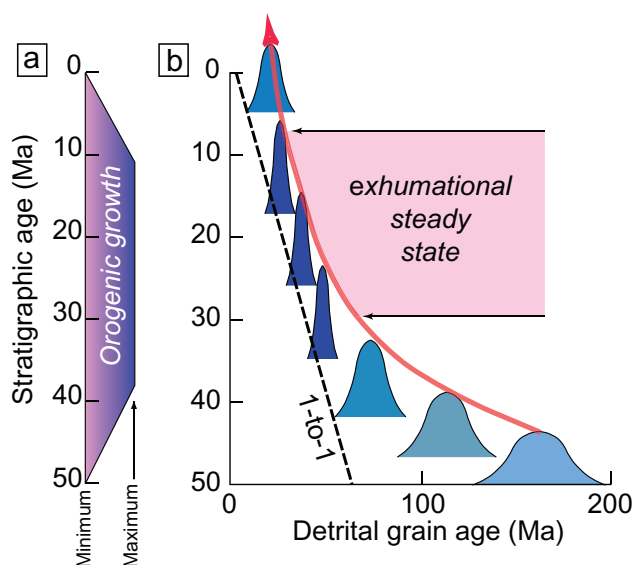


Fig. 8 Relationships among orogenic growth, populations of detrital cooling ages and lag times. (a) Orogenic growth during constructional (40–50 Ma), steady-state (10–40 Ma) and destructional (0–10 Ma) phases. (b) Theoretical sequence of populations of detrital cooling ages represented by Gaussian distributions of ages. The lag time represents the difference between the peak of the cooling age distributions and the stratigraphic age. The 1-to-1 line occurs where the detrital age and the stratigraphic age are equal. Detrital age populations that fall on this line represent a lag time of 0 Myr. During constructional phases, lag times decrease as erosion proceeds increasingly deeply into the hinterland. Lag times remain constant during exhumational steady state and increase again during the destructional phase as orogenesis and erosion rates wane.

Although a spectrum of cooling ages from a given orogen is typically measured in a single sedimentary sample, the distribution of ages is commonly deconvolved into a small number of component populations (Brandon, 1992) that, when summed together, approximate the observed age distribution. The time difference between the youngest component peak of the detrital ages and the depositional age is used to define the lag time (Garver & Brandon, 1994).

Consider the growth and decay of an orogen over 50 Myr (Fig. 8). During its initial growth, the detrital ages are old, but the lag time becomes progressively younger. During steady state, a constant lag time is displayed, and this interval of the shortest lag times equates with the most rapid

erosion. During a waning stage of orogenesis, lag times should increase, but not as rapidly as they decreased in the initial growth stages, because in the post-orogenic stage, many minerals that have recently passed through their closure temperature will be exhumed.

Irrespective of considerations of orogenic steady state, the abrupt appearance of a suite of younger detrital ages within a stratigraphic sequence could be interpreted to define or slightly post-date the onset of deformation in the hinterland (as long as the change has not resulted from capture of a new source area). Detrital ages can also be used as a provenance tracer with respect to tectonic reconstructions: exposure of a new source area with a distinctive suite of cooling ages, even very old ones (Carter & Moss, 1999), can provide a readily discernible detrital signal to a nearby basin. Finally, detrital ages can be used to place useful limits on poorly dated continental strata. For example, the occurrence of detrital grains with cooling ages younger than the previously assigned depositional age can force upward revisions in the depositional age (Najman *et al.*, 2001).

TESTING THE FIDELITY AND SENSITIVITY OF DETRITAL AGES

Each of the interpretive strategies or applications described above relies on the assumption that the detrital signal in a basin provides a faithful representation of the age distribution in the hinterland source area (Garver *et al.*, 1999). For fission-track dating in deep sedimentary basins, this assumption is commonly violated due to burial heating that partially or fully resets fission-track ages, especially for apatite grains (Green *et al.*, 1989). Zircon fission-track ages are less susceptible to resetting due to their higher closure temperature, but given this higher temperature they are also relatively insensitive to exhumation that is < 5–8 km. Hence, when applying fission-track dating to detrital samples, the likely thermal history of the depositional basin from which samples are collected and the magnitude of hinterland exhumation should dictate whether apatite or zircon is dated.

Even in the absence of reset ages, the correspondence between observed detrital ages and bedrock ages in their source area is rarely assessed. For

example, muscovite is a typical mineral exploited for single-crystal detrital dating, and yet the platy nature of muscovite's mineral habit would seem to make it particularly susceptible to comminution during transport. Consequently, any downstream changes in populations of detrital muscovite ages might be an artefact of the loss of grains from farther upstream, rather than an indication of downstream changes in erosion rates and cooling ages. In this case, downstream changes in populations of ages would provide scant insights on variable erosion rates. On the other hand, if muscovite were to travel primarily in a river's wash load, it could experience only minor comminution through grain-to-grain collisions, such that observed detrital ages would be independent of transport distance. One way to test whether comminution is likely to have modified age distributions is to compare detrital age populations of minerals with different susceptibilities to comminution, but collected from the same site. For example, micas are highly susceptible to comminution, whereas zircon is resistant. If, using dating methods with comparable closure temperatures, the distribution of ages from muscovite and zircon are similar at the same site, this would argue against transport distance or comminution as an important control on observed ages.

When 55 $^{40}\text{Ar}/^{39}\text{Ar}$ muscovite ages (closure temperature: ~ 350°C) and 70 zircon fission-track ages (closure temperature: ~ 250°C) are compared from the same site in a Himalayan river ~ 150 km below its headwaters, the populations of ages resemble each other, although the primary peak in the zircon age population is shifted 1–2 Myr younger in comparison to the muscovite ages (Fig. 9). In fact, such a shift is expected, given the lower closure temperature of zircon fission-track ages. This example suggests, therefore, that the detrital age signal of muscovite can yield a reliable proxy for the distribution of cooling ages in the entire upstream catchment and that comminution during transport creates only minor perturbations.

Detrital age studies assume that meaningful errors can be assigned to dates for individual grains. Most of the detrital studies published to date have utilized zircon fission-track, $^{40}\text{Ar}/^{39}\text{Ar}$ and U–Pb dating of single crystals, because the uncertainty on any single-crystal age is commonly small. The U and Th content of apatite, however, is typically an order of magnitude less than that of

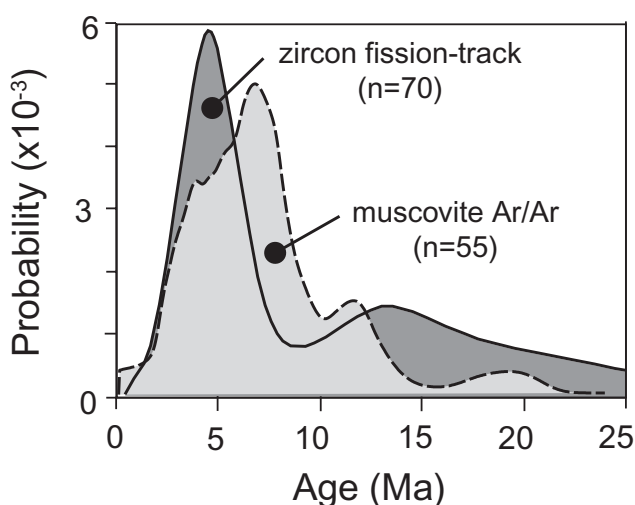


Fig. 9 Comparison of the age distribution of a resistant mineral (zircon) and a mineral susceptible to comminution (muscovite), to assess whether downstream transport causes selective loss of non-resistant minerals. In this example, zircon and muscovite were separated from detrital sand samples collected at the same site and were dated by fission-track (closure temperature $\sim 240^{\circ}\text{C}$) and $^{40}\text{Ar}/^{39}\text{Ar}$ (closure temperature $\sim 350^{\circ}\text{C}$) methodologies, respectively. The basic patterns of detrital ages are in agreement, but the zircon ages are shifted ~ 2 Myr younger. This shift is expected, given the lower closure temperature of zircon. The overall similarity of the age spectra, including the 2-Myr shift, suggests that, despite having been collected over 150 km from the headwaters, the muscovite ages have not experienced significant attrition. This lends support to arguments that micas travel largely in the wash load where little loss occurs due to comminution.

zircon. As a consequence, fewer fission tracks are generated, and even the best of apatite fission-track bedrock samples will have a distribution of grain ages that is dispersed around the 'true' cooling age. The implication of this inherent age uncertainty for detrital studies is that it is difficult to assign an uncertainty to individual grain ages beyond the uncertainty based on the counting statistics, and yet the expected uncertainty would be considerably larger. As a consequence, the approach most commonly used for interpreting detrital fission-track data is to determine the statistically significant component populations that can be arithmetically combined to yield the observed distribution of detrital ages (Brandon, 1992; Brandon & Vance, 1992).

Detrital ages of individual crystals are also typically assumed to be independent of grain size. As

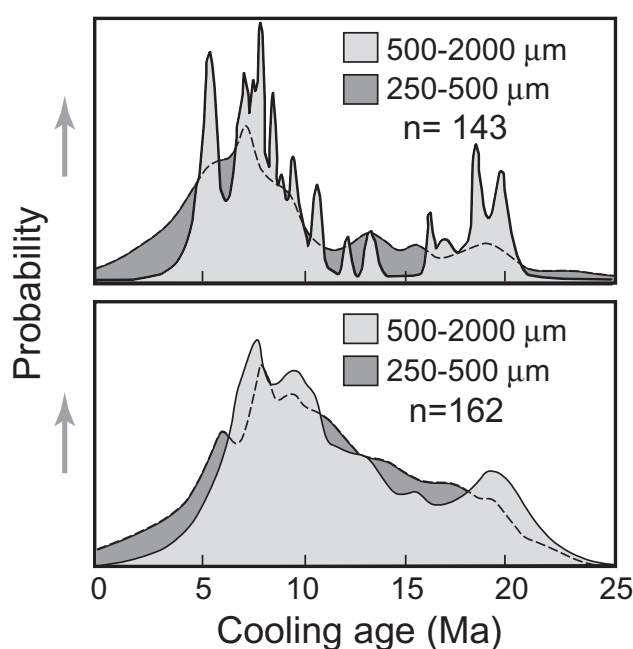


Fig. 10 Comparisons of detrital muscovite $^{40}\text{Ar}/^{39}\text{Ar}$ ages for different size fractions in the same sample at two different sites in the Marsyandi catchment, central Nepal. The composite probability curve is constructed by summing up individual grain-age measurements by assigning each age a Gaussian 'kernel' with an area equal to unity, a width that is defined by the uncertainty on the age, and a most probable age that equals the measured age. The summed probability of all grains is then re-normalized to unity. Overall, the distributions of ages are independent of grain size, suggesting a similar spatial distribution and susceptibility to erosion for both size ranges in each catchment. The less peaked nature of the probability curve for the smaller grain sizes in the upper sample is due primarily to the higher analytical uncertainties associated with small grains with young cooling ages. (Modified from Ruhl & Hodges, 2005.)

a consequence, grain sizes that are most amenable to a given dating approach are commonly analysed. For example, because recently cooled muscovite grains contain only small quantities of radiogenic argon, large detrital grains ($> 500 \mu\text{m}$) are typically dated in order to minimize the error on each age. Comparisons of single-grain age distributions (Ruhl & Hodges, 2005) can show similar age distributions for different size fractions at a given site (Fig. 10) that validate the assumed size independence of ages. In these situations, the distribution of grain sizes in contributing areas with different cooling histories must remain fairly uniform. On the other hand, if all of the fine-grained muscovite occurred

in a rapidly eroding area, whereas the coarse-grained muscovite derived from a slowly eroding domain, then analysis of only the coarse fraction would miss the young, rapidly cooled grains. Thus, if schists and granites experienced different erosion rates, analysis of coarser muscovite grains might only reflect the cooling history of the granite.

The distribution of detrital ages in a river is assumed to be unchanging at annual time-scales and homogeneous at spatial scales of tens of metres. It is commonly assumed that sampling in the spring or autumn would not change the observed age distribution. Similarly, grab samples from different positions on a gravel bar are assumed to yield comparable detrital ages. Such assumptions are infrequently tested, yet one can envision circumstances that would create instability in the detrital age signal: large landslides in a given catchment; different, seasonally dependent erosion mechanisms or sediment transport events in different catchments (glacial meltwater versus winter rainstorms); preferential storage of some sediments; or different grain sizes from different catchments that are hydraulically sorted into different positions on a bar. For example, Amidon *et al.* (2005a) found > 50-fold differences in zircon abundance for different size fractions at the same site. In stratigraphic studies of detrital minerals, the cost and labour of dating individual grains typically precludes testing of duplicate samples separated laterally by tens of metres or vertically by centimetres. Nonetheless, such tests are needed to verify the stability (or arbitrariness) of the detrital signal (see Ruhl & Hodges (2005) for examples of time-varying distributions).

Dated grains from detrital samples are assumed to provide a reliable portrait of the population of grain ages. Only a limited number (40–100) of grains are typically dated, however. For a simple distribution of grain ages, such as when a single dominant age peak is present, 40 dates are sufficient to capture its essential characteristics. For distributions with multiple peaks, 100 dates may only begin to mimic the true complexity of the age distribution (Brewer *et al.*, 2003; Vermeesch, 2004). Although dating larger numbers of grains is perhaps the most reliable means to address this issue, numerical smoothing of age distributions improves the match between ‘daughter’ and ‘parent’ distributions, especially for complex age distributions (Amidon *et al.*, 2005b). The technique of extracting

component age peaks from the observed distributions also serves as a smoothing function (Brandon, 1996, 2002) that reduces mismatches.

Despite a common desire to extract as much detailed information as possible from detrital age data, the sensitivity of detrital ages to small changes in the magnitude or rate of erosion has rarely been well assessed. To evaluate this sensitivity, apatite fission-track ages from the Kyrgyz Range in the northern Tien Shan provide a test case. Here the distribution of bedrock cooling ages is particularly well documented (Sobel *et al.*, 2006) and differences of 1–2 km in differential erosion along the length of the range can be discerned. Two previous studies by Bullen *et al.* (2001, 2003) in the Ala Archa catchment (central Kyrgyz Range) have demonstrated the presence of an exhumed partial annealing zone and of an underlying zone of reset ages where, throughout a zone > 1 km thick, all of the apatite ages are ~ 11 Ma (Fig. 11a–d). The kink in the age–elevation trend at the base of the exhumed partial annealing zone has been interpreted to represent the time at which rock uplift and erosion accelerated (see Fig. 2 for the conceptual background) in the Kyrgyz Range following a 100-Myr-long interval of quiescence and slow erosion (Bullen *et al.*, 2003). Along the sampled bedrock transect (Fig. 11d), the oldest ages are ~ 20 Ma (~ 4000 m elevation) and lie well within the partial annealing zone (Fig. 11d). The catchment containing this transect, however, extends deeper within the range, where, given a southward tilt of the range that is imposed by the north-vergent thrusts beneath it, still older cooling ages are expected to be prevalent.

With this known ‘stratigraphy’ of cooling ages, it becomes possible to assess whether a catchment yields ages of a predictable range and abundance (Stock & Montgomery, 1996). Following the logic of Brewer *et al.* (2003), it would be predicted that the relative frequency of ages should result directly from convolving the hypsometry of the catchment (Fig. 5) with the cooling age ‘stratigraphy’. To test this concept, detrital apatites were dated in a sample of sand from the modern Ala Archa River, which drains the catchment that encompasses the bedrock transect. The youngest age component of the detrital sample displays a peak of 17 ± 2 Ma (Fig. 11e) and is highly consistent with the detrital ages that would be expected, given the observed altitudinal distribution of cooling ages (Fig. 11d).

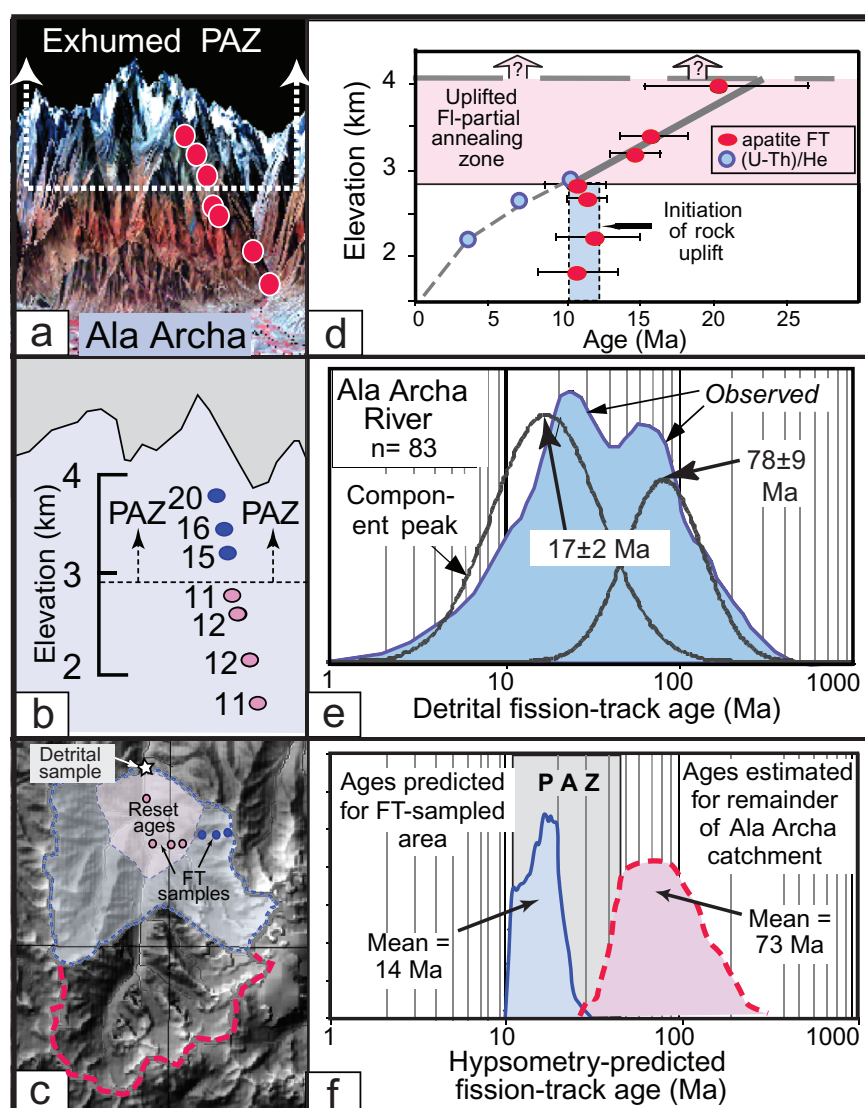


Fig. 11 Bedrock and detrital apatite fission-track ages from Ala Archa, central Krygyz Range, Tien Shan. (a) Vertically exaggerated DEM draped with a satellite image and showing location of fission-track samples. Dark circles lie beneath the exhumed partial annealing zone (PAZ). (b) Cooling ages (Ma) in their relative vertical positions. (c) Digital elevation model showing the location of the bedrock samples (coloured dots), detrital sample (star) and the outline (blue dashed line) of the northern part of the Ala Archa drainage containing the FT samples, and the southern part of the catchment (red dashed line). (d) Age–elevation profile depicting the base of the PAZ and indicating an age of 11 Ma for the beginning of rapid cooling and rock uplift. (e) Detrital FT data from modern sand in Ala Archa River, showing two component populations that account for most of the observed distribution. The mean of the younger population appears consistent with the observed FT relief section. (f) Computed distributions of FT ages for the Ala Archa catchment based on the areas outlined in (c). The younger population results from convolving the hypsometry with the predicted age–elevation trend (d) and provides a close match to the observed 17 ± 2 Ma population. The older population is calculated assuming the PAZ is tilted southward at $\sim 12^\circ$ and that the age–elevation trend in the PAZ remains similar to the observed trend (d). The shaded ‘PAZ’ area indicates all samples derived from within the PAZ.

When the altitude-dependent cooling ages are combined with the hypsometry of the northern Ala Archa sub-basin from which the samples were collected (Fig. 11c), the resulting distribution of ages yields an average age of 14 Ma (Fig. 11f) and provides a rather good match to the younger component peak in the observed detrital ages (Fig. 11e).

Not unexpectedly (given the young bedrock cooling ages: Fig. 11d), these predicted ages fail to match the older observed ages with a component age peak at ~ 80 Ma, which are probably derived from the more southerly part of the catchment. To mimic this older age component, it is suggested that the range has been tilted southward at $\sim 12^\circ$, such that the base of the partial annealing zone is located below 1600 m altitude in the southern part of the catchment. To obtain a satisfactory match to the older (80 Ma) observed age peak (Fig. 11e), a much larger range of bedrock ages is required. Therefore, above the PAZ, a strong altitude dependency is required to produce ages ranging from Tertiary to Palaeozoic. Although the overall match to the observed ages is inexact, this hypsometric approach mimics the observed data and provides some insight into the age distribution in the bedrock. In particular, in order to produce the observed ages, it requires that unsampled, southern parts of the catchment have much older cooling ages than those observed in the fission-track vertical transect. Overall, this analysis suggests that the detrital ages provide a high-fidelity record of the bedrock cooling ages in the tributary catchment.

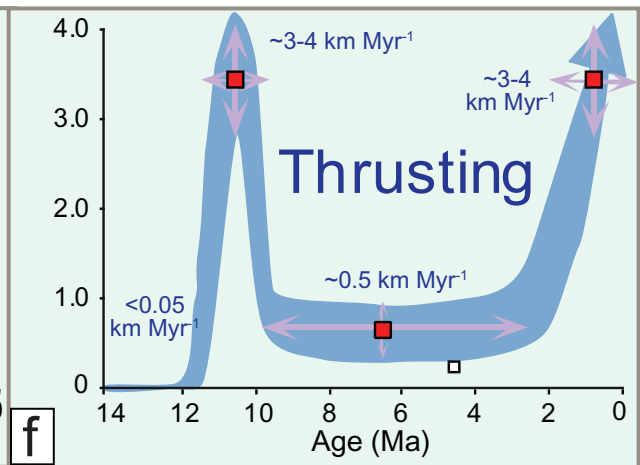
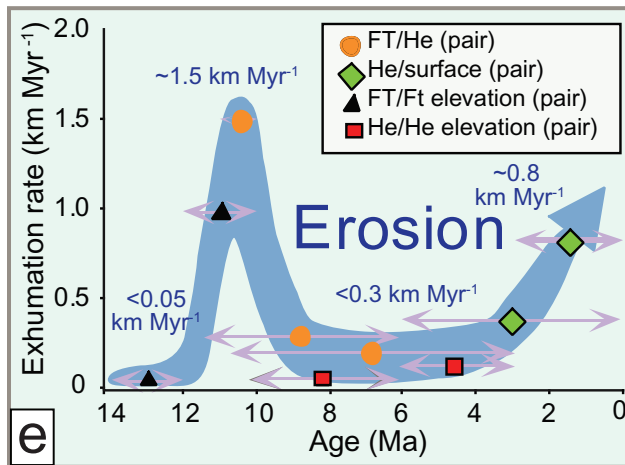
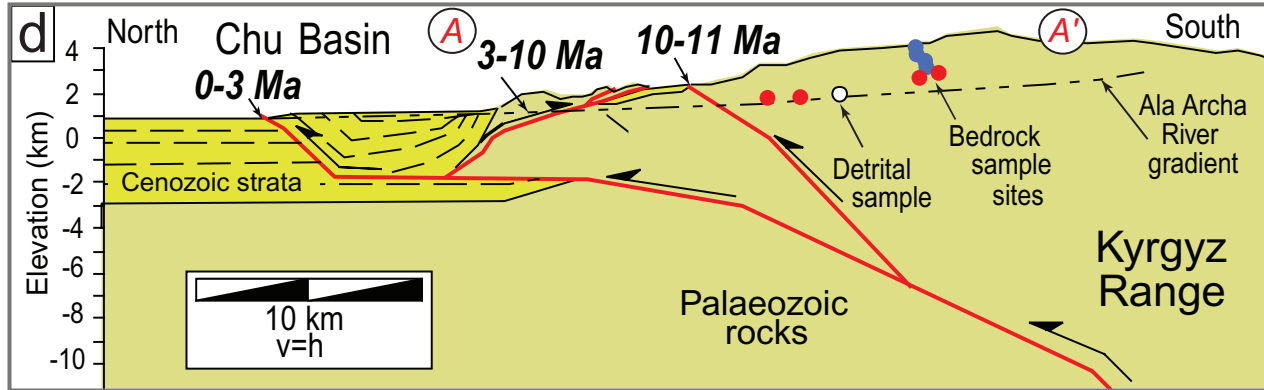
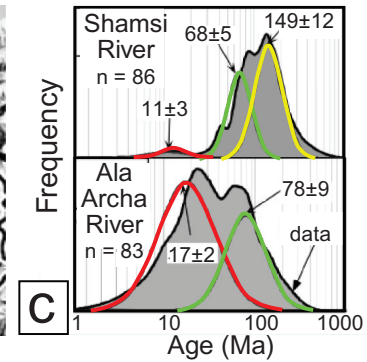
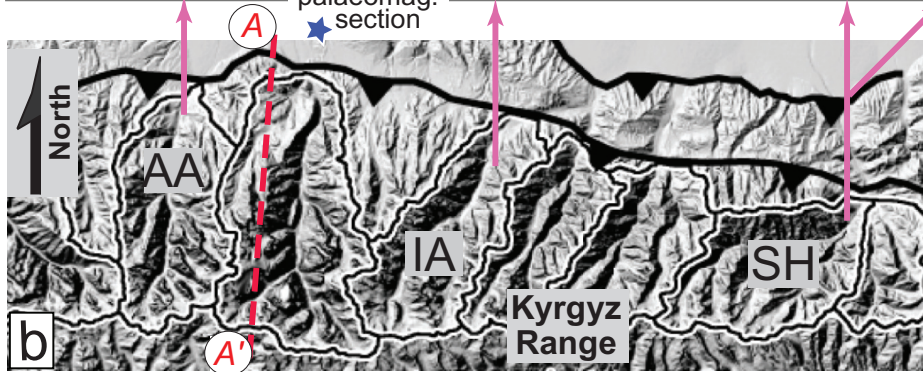
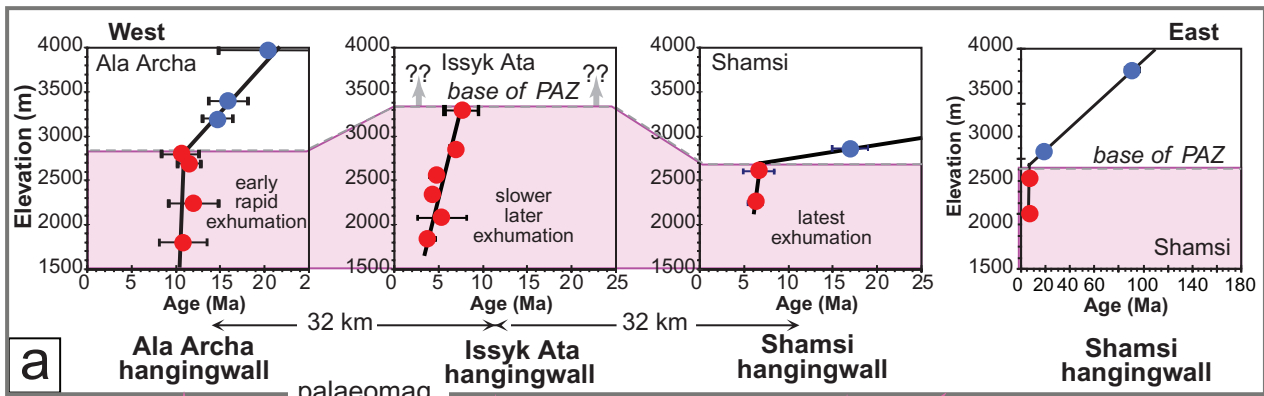
Along the trend of the Kyrgyz Range, two additional vertical relief sections of apatite ages have been analysed (Sobel *et al.*, 2006). Together, the three sections span about 60 km laterally (Fig. 12b) and display consistent trends of young ages at the lowest altitudes and older ages higher up (Fig. 12a). From east to west, however, the altitude of the top and base of the partial annealing zone varies significantly. For example, at 2800 m in the east at Shamsi, a cooling age of ~ 17 Ma occurs within the PAZ (Fig. 12a), whereas at the same altitude farther west, fully reset cooling ages of ~ 7 Ma and ~ 11 Ma occur beneath the PAZ in the Issyk Ata and Ala Archa sections. At 3800 m, samples from all three sections lie within the PAZ, but also show a strong east–west gradient, ranging from ~ 70 Ma in the east to ~ 18 Ma in the west at Ala Archa. The height of the base of the PAZ is greatest in the Issyk

Ata drainage (Fig. 12a), thereby suggesting that more erosion and rock uplift have occurred here. The oldest ages occur at Shamsi, where the onset of rapid cooling (~ 7 Ma) appears later than at the other sites and the total magnitude of erosion appears to be the least.

If detrital samples faithfully reflect the cooling ages in their source rock, these along-strike fission-track profiles should provide a test to discern the sensitivity of modern samples to the bedrock ages in their source areas. Indeed, the contrast between samples from the modern Shamsi and Ala Archa Rivers (Fig. 12c) is striking. In Shamsi, only a very small representation exists of ages < 17 Ma, whereas the dominant component peaks are ~ 70 Ma and ~ 150 Ma, more than 50 Myr older than the dominant peak at Ala Archa. In both cases, the detrital ages are highly consistent with the observed bedrock cooling ages (Fig. 12a). Moreover, the contrast in the primary age component suggests that, under appropriate circumstances, detrital fission-track ages can resolve differences on the order of 1–2 km in the magnitude of erosion between different sections.

When combined with geological data (Bullen *et al.*, 2003), the known bedrock-cooling ages from the Kyrgyz Range also underpin a reconstruction of the sequential dissection of the range that is based on detrital fission-track ages. Prior to deformation beginning at ~ 11 Ma, the region was characterized by rocks with Mesozoic and late Palaeozoic cooling ages that extended from the surface to the top of the PAZ, yielding a vertical succession of ages (cf. Fig. 7). After rock uplift commenced in the late Middle Miocene, accelerated erosion created an enhanced sediment flux to the nearby Chu basin, the Cenozoic foreland basin that bounds the northern margin of the Kyrgyz Range.

Based on a magnetostratigraphic section that provides time control from ~ 9 Ma to 3 Ma (Bullen *et al.*, 2001), four different stratigraphic horizons, ranging from 8.5 Ma to ~ 1.5 Ma, were analysed for detrital apatite fission-track ages (Fig. 13). Even though the oldest stratigraphic sample was collected from strata that post-dated the initiation of uplift by some 2–3 Myr, the youngest component of its detrital ages is centred at ~ 165 Ma and contains no post-Mesozoic ages. This absence indicates that erosion at this time had not progressed into the former partial annealing zone (Fig. 7). Within



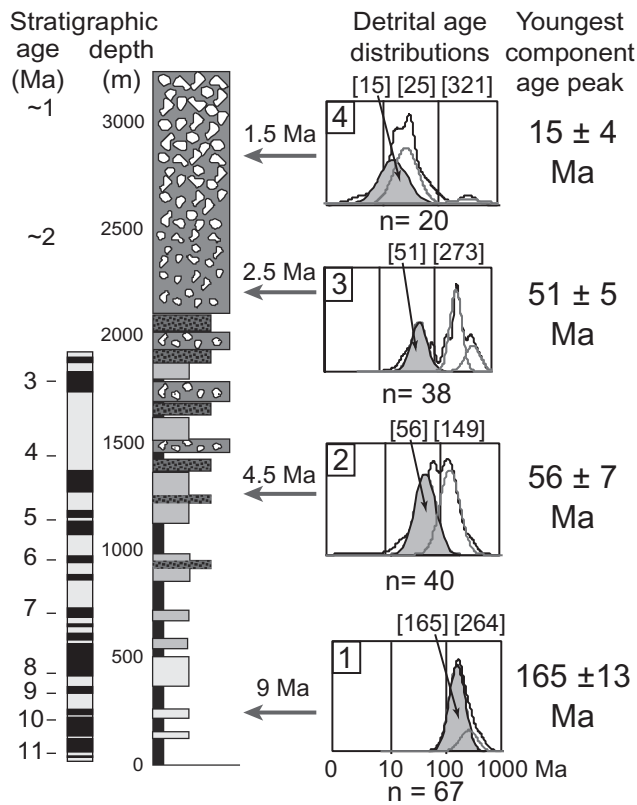


Fig. 13 (left) Detrital fission-track data at four stratigraphic horizons in the Chu basin. Section lies in the foreland of the Kyrgyz Range, offset 15 km east from the outlet of the Ala Archa catchment (star, Fig. 12b). Stratigraphic time control derives from magnetostratigraphy (Bullen *et al.*, 2001). Grain-age populations, or peaks (labelled in Ma), were statistically separated using the binomial peak-fitting routine of Brandon (1996). Youngest peaks at each level (shaded grey) decrease in age up-section from 165 Ma to 56 Ma, then 51 Ma and finally to 15 Ma at 9, 4.5, 2.5 and 1.5 Ma, respectively. The large change in detrital ages from 9 to 4.5 Ma suggests that erosion progressed into the partial annealing zone (PAZ) during this interval. The very small change in ages between 4.5 and 2.5 Ma suggests that hinterland erosion was slow during this interval and remained within the PAZ, whereas the young ages from 1.5 Ma indicate erosion has proceeded well into the zone of reset ages. This youngest age peak (~15 Ma) is indistinguishable from the analogous peak in the modern Ala Archa River (17 Ma: Fig. 11f), suggesting exhumational steady state. The small change in detrital ages between 4.5 and 2.5 Ma indicates very limited erosion during this interval and is synchronous with slower rates of erosion and shortening in the hinterland (Fig. 12e, f).

the next 4 Myr, an abrupt change in detrital ages is manifested (Fig. 13), as the youngest component peak drops to ~55 Ma. Given the absence of significant thermal events affecting this region in Cenozoic times, the presence of Cenozoic detrital ages clearly indicates that the PAZ had been

breached by 4.5 Ma. Over the next 2 Myr, the youngest component age peak remains almost constant (50–55 Ma). The persistence of a peak of nearly the same age can be interpreted to indicate that the rate of erosion decreased, because no significantly younger ages from greater depths in the nearby hinterland were being introduced to the

Fig. 12 (opposite) Bedrock and detrital cooling ages from multiple, along-strike sites in the Kyrgyz Range, northern Kyrgyzstan. (a) Vertical apatite fission-track sections from the central (Ala Archa) to the eastern (Shamsi) Kyrgyz Range. All three sections contain some completely reset cooling ages near the base, but pronounced differences occur in ages within and adjacent to the PAZ at a given elevation, and the base of the PAZ occurs at different elevations, thereby indicating variable amounts of rock uplift and erosion. Note two depictions of the Shamsi data (right) with different age scales. (b) Shaded relief map of the Kyrgyz Range, showing catchments where bedrock and modern rivers were sampled. Star marks location of magnetostratigraphic section. AA, Ala Archa; IA, Issyk Ata; SH, Shamsi. (Modified after Sobel *et al.*, 2006.) (c) Modern detrital apatite fission-track ages from the Shamsi River (top) and Ala Archa (bottom) clearly capture the differences in the cooling age stratigraphy in the catchments from which they were derived. (From Bullen *et al.*, 2001.) (d) Simplified geological cross-section of the central Kyrgyz Range showing major forethrusts and backthrusts, plus locations of vertical-relief bedrock samples and detrital fission-track sample. (From Bullen *et al.*, 2003.) The interval of primary displacement on each major fault is indicated. Location of the central part of the cross-section (A-A') is shown in (b). (e) Summary of punctuated rates of erosion deduced from bedrock cooling ages in the central Kyrgyz Range near Ala Archa. Various combinations of data are used to define rates, such as the elevation difference between two samples divided by the difference in their ages. The fast-slow-fast pattern of erosion is consistent with the changes in populations of detrital ages from these same time intervals in the stratigraphic record (Fig. 13). (Modified from Bullen *et al.*, 2003.) (f) Variations in shortening rates through time deduced from structural cross-section at Ala Archa and ages assigned to faulting episodes. Note the overall temporal concurrence with the erosion rate changes (e). (Modified after Bullen *et al.*, 2003.)

foreland. This is consistent with the record of hinterland erosion as deduced from (U–Th)/He bedrock cooling ages (closure temperature $\sim 70^\circ\text{C}$: Farley, 2000; Fig. 11) and structural analysis (Fig. 12d) that shows a threefold decrease in the rate of shortening, erosion and rock uplift between 8 Ma and 2 or 3 Ma (Fig. 12e, f), when compared with deformation and erosion between 10 and 12 Ma (Bullen *et al.*, 2003). The youngest detrital sample at 1.5 Ma shows another abrupt decrease in the age of its youngest component peak. In fact, its ~ 15 Ma age is indistinguishable from the 17-Ma peak seen in the modern Ala Archa River (Figs 11 & 13). These young ages indicate that erosion had progressed through the exhumed PAZ and into the zone of reset ages that is presently exposed at elevations < 2800 m (Fig. 11d). This inference is also consistent with the (U–Th)/He dates, which require erosion to exhume rocks from depths of ~ 3 km in the past 3 Myr (Fig. 11). In sum, over the 8-Myr-long stratigraphic record of detrital ages, the youngest component age peak decreased by ~ 150 Myr, and hinterland incision (as inferred from the pre-erosion hinterland age stratigraphy) totalled ~ 5 – 6 km. The decreasing lag time (Fig. 8) clearly indicates that the range had not attained an exhumational steady state until at least Pleistocene times.

This succession of detrital age samples aptly illustrates progressive hinterland unroofing. Such an analysis of detrital ages is clearly strengthened by the documented cooling-age stratigraphy of the bedrock in the hinterland (Figs 8 & 11) that permits quantification of the approximate magnitude of erosion at each time step recorded by the foreland-basin samples. Even in the absence of documentation of the hinterland age stratigraphy, robust inferences can be drawn on the magnitude of erosion from the component ages in each depositional level in the basin. For example, the initial appearance of sediments that were eroded from the PAZ is clearly evident, and changes in relative rates of erosion can be estimated from the persistence or changes in component ages from one depositional level to the next (Fig. 8).

EVOLUTION OF DETRITAL AGES THROUGH AN ACTIVE OROGEN

The detrital minerals that are preserved within basinal strata contain a final amalgam of ages that

emerged from the hinterland. The way in which that detrital signal is created within the hinterland, however, typically remains unknown and, thereby, leaves unresolved questions. What combination of tectonic, lithological and erosional controls determines the suite of minerals and cooling ages that are transported out of the hinterland? How do spatial variations in erosion rates or lithology in the hinterland affect the downstream evolution of the suite of detrital ages? Although few studies have examined the downstream evolution of detrital cooling ages within a hinterland (Bernet *et al.*, 2004a; Brewer *et al.*, 2006), the expectation is that regions within the hinterland with rapid erosion rates, high abundances of the target mineral, and large areas will dominate the detrital age signal.

To test these expectations and to document the evolution of the detrital age signal through an active orogen, over 400 muscovite grains have been analysed from 11 sites along the Marsyandi River in central Nepal (Brewer *et al.*, 2006). This catchment extends from the southern edge of the Tibetan Plateau to the Gangetic foreland (Fig. 14a). Along its course, the river flows across both the South Tibetan Detachment fault, a down-to-the-north normal fault, and the Main Central Thrust fault, a major south-vergent thrust fault (Hodges, 2000). These two faults bound the Greater Himalaya, which contains about one-third of the Marsyandi catchment. Another third lies in the Tethyan strata of Palaeozoic age associated with the Tibetan Plateau, and the remainder lies within Lesser Himalaya, south of the Main Central Thrust. If all three subcatchments had similar hypsometries and distributions of muscovite and were eroding at the same rate, no downstream changes in detrital ages would be anticipated.

Quite expectedly, however, the detrital age signal changes dramatically downstream (Fig. 14b & c). The sample highest in the catchment has over 80% of its source area in Tethyan rocks (Site 11, Fig. 14a). Its detrital ages display a strong peak centred at ~ 14 Ma. Only 20 km farther downstream (Site 10, Fig. 14b), the 14-Ma peak has nearly disappeared and has been replaced by a 17–18-Ma peak. Such a change leads to an apparent contradiction: the dominance of the older, 17–18-Ma peak suggests that it derives from a region that is supplying more sediment to the trunk stream, whereas the fact that the dominant age is becoming older downstream

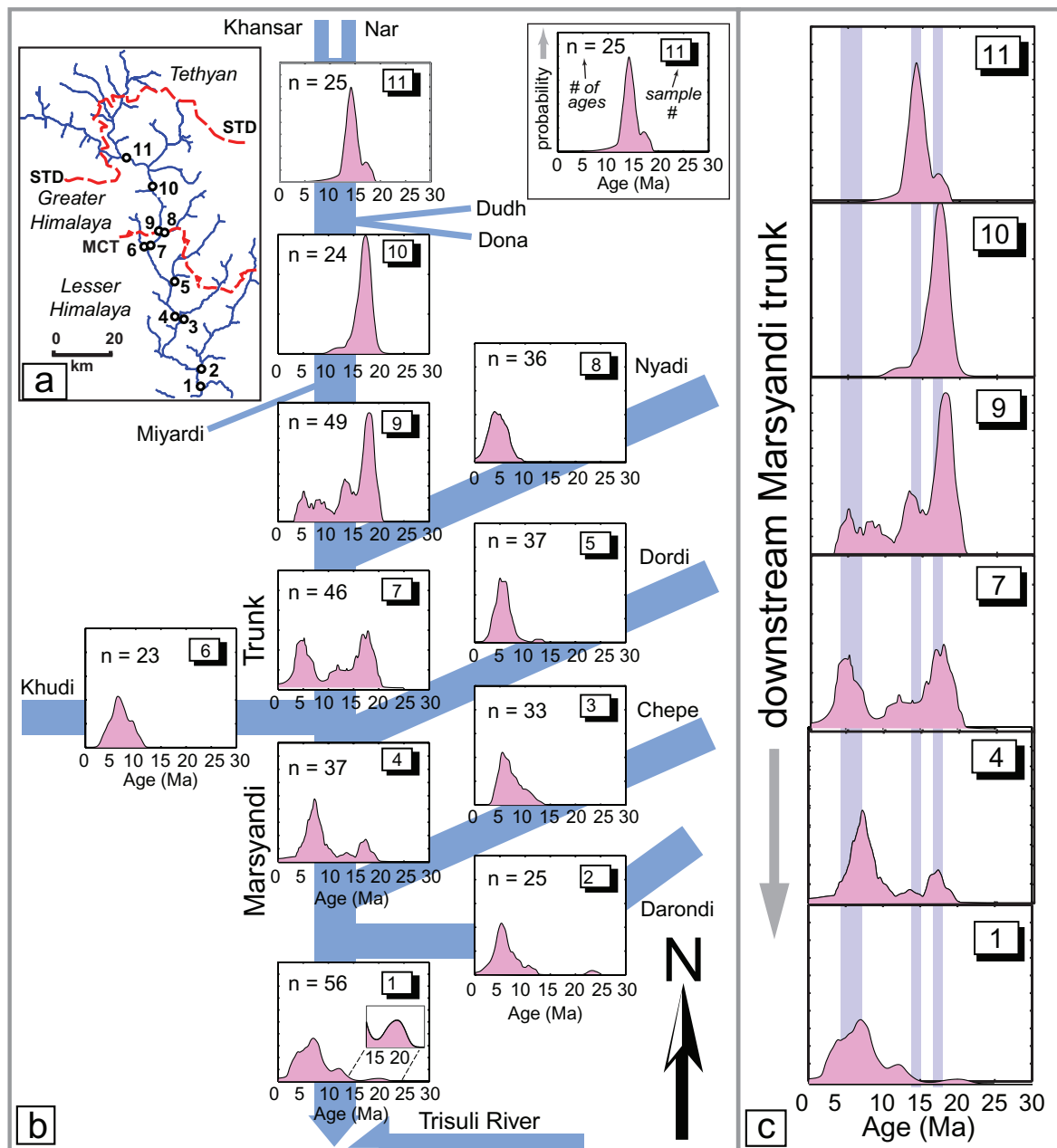


Fig. 14 Detrital muscovite $^{40}\text{Ar}/^{39}\text{Ar}$ ages along the Marsyandi River, central Nepal. (a) With headwaters in the Tibetan Plateau, the Marsyandi traverses the Greater and Lesser Himalaya. Numbered sample locations for both trunk stream and major tributaries are shown. STD, South Tibetan Detachment (down-to-the-north normal fault); MCT, Main Central Thrust. (b) Topological map of the Marsyandi drainage showing probability density functions of detrital muscovite ages at each sample site. Ages are smoothed with a 2-Myr scrolling window. Downstream changes in age distribution reflect contributions due to catchment erosion rate, size and lithology. Note that the northern sites have older cooling ages, southern tributaries show young (< 10 Ma) ages, and the sample at the mouth (Site 1) contains few of the older ages that are abundant in the headwaters. These data suggest that an influx of younger ages from tributaries in the lower part of the catchment overwhelms the older ages that characterize the headwater region of the catchment. (c) Downstream changes in cooling ages along the main stem of the Marsyandi River. Shaded bars indicate the approximate age range for prominent detrital age peaks that vary in significance along the Marsyandi's course. (Modified after Brewer *et al.*, 2006.)

implies slower erosion rates. These observations can be reconciled by the fact that muscovite is 5–10 times more abundant in the tributaries emerging within the Greater Himalaya (Brewer *et al.*, 2006). The resultant flux, despite somewhat slower erosion rates (Fig. 6), could cause the Greater Himalayan signal to overwhelm that from the upstream mica-poor Tethyan regions (Fig. 14c).

As the Marsyandi traverses the Greater and then the Lesser Himalaya, two significant trends emerge within the detrital age data. First, the 17–18-Ma peak which is so dominant high within the Himalaya has almost disappeared when the Marsyandi debouches into the Trisuli River: a trans-Himalayan river with a considerably larger catchment. Second, a peak with ages concentrated in the 5–8-Ma range becomes increasingly important downstream. The reason for the emergence of the 5–8-Ma peak becomes clear when the age signal from the major tributaries is examined: all of them are dominated by the same 5–8-Ma peak and contain almost no ages older than ~12 Ma (Fig. 14b). These younger ages indicate more rapid erosion in these tributaries, and their muscovite fraction is also another three to ten times higher than in the Greater Himalayan tributaries that feed Site 10 (Brewer *et al.*, 2006).

Several clear conclusions can be drawn from this analysis of modern detrital age samples. First, the detrital signal that is delivered from a mountain range to an adjacent basin is commonly transformed along its passage through the mountains. If the foreland basin were closer to the upland area (in this case, the Tibetan Plateau), a very different detrital age spectrum would be present. Second, shifts toward younger detrital ages typically reflect higher rates of erosion for catchments contributing the younger ages (Fig. 6). Third, at the scale of tributary catchments, the abundance of the target mineral (in this case, muscovite) can change by an order of magnitude or more across a few tens of kilometres. Interpretations offered by studies that assume the distribution of a target mineral is uniform (Bernet *et al.*, 2004a) may need modification when the actual distribution of the target mineral is known.

The available detrital age data make it possible to estimate erosion rates in each of the tributary catchments (Brewer *et al.*, 2006), given several assumptions and observations. It is assumed that: (i) within a given tributary, erosion rates and

muscovite distributions are approximately uniform; (ii) there is no significant relief on the 350°C isotherm – an assumption consistent with topographic relief of ≤ 6 km and erosion rates ≤ 3 mm yr⁻¹ (Fig. 3); (iii) rock-particle trajectories are vertical. If true, then the altitude dependence of the distribution of ages can be predicted for any erosion rate (Fig. 5). Combining these ages with the observed catchment hypsometry yields a prediction of detrital ages (Fig. 5). The optimal erosion rate for each tributary catchment is calculated by minimizing the mismatch between the predicted and observed distributions of detrital ages (Brewer *et al.*, 2003).

The resultant map of variations in predicted erosion rates at the catchment scale depicts regional trends across the Himalaya (Fig. 15). The calculated rates vary from 2.3 mm yr⁻¹ to 0.9 mm yr⁻¹ with higher rates along the southern flank of the Himalaya than along the northern flank. The highest rates occur in the Nyadi to Darondi catchments, each of which straddles the Main Central Thrust. Strikingly, those catchments that include the highest Himalayan topography (e.g. Dona, Dudh and Khansar) have significantly lower erosion rates. These spatial variations indicate that, at the present time, the most rapid erosion is displaced well south of the Himalayan crest. Such a position coincides spatially both with the swath of highest monsoonal precipitation (Burbank *et al.*, 2003) and with the zone adjacent to and immediately south of the Main Central Thrust, where young bedrock-cooling ages (Harrison *et al.*, 1998), steepened stream gradients (Wobus *et al.*, 2003) and brittle faulting (Hodges *et al.*, 2004) suggest active deformation.

DETRITAL AGES AND COLLISIONAL TECTONICS

Most studies that attempt to convert cooling ages into erosion rates consider only the vertical transport of rocks toward the surface (e.g. Stüwe *et al.*, 1994; Fitzgerald *et al.*, 1995; Garver *et al.*, 1999). Such vertical kinematics were used in the previous estimates of Himalayan erosion rates (Figs 3, 6 & 15) described above (Brewer *et al.*, 2006). Yet, in most convergent orogens rock primarily advects laterally, not vertically, such that convergence is commonly five to ten times greater than vertical rock uplift (Willett, 1999; Stüwe & Hintermüller, 2000; Batt & Brandon, 2002). Rocks with different thermal

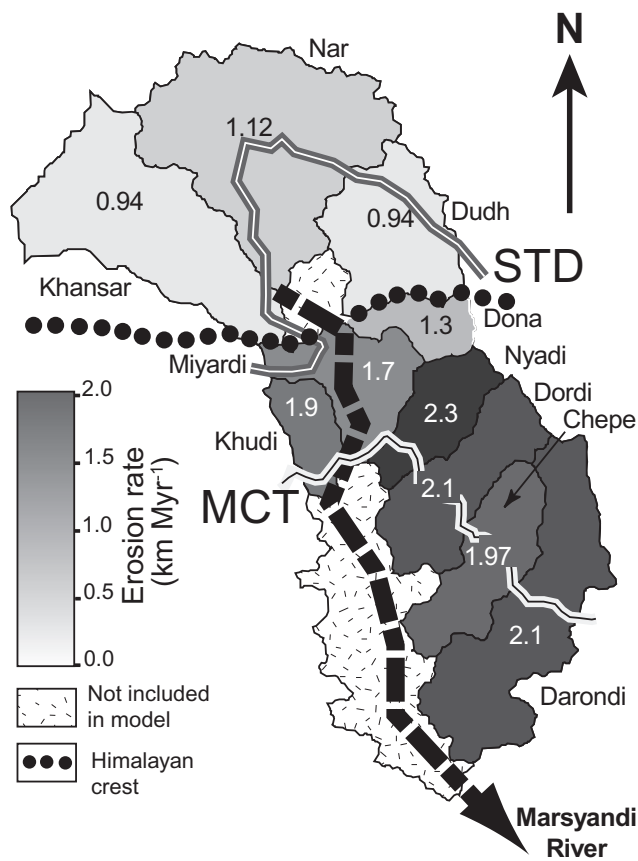


Fig. 15 Spatial variation in erosion rates at the catchment scale for the Marsyandi River. Erosion rates are taken from the results of modelling the detrital cooling-age probability density distributions for individual tributaries. The stippled areas indicate zones not included in the calculations and the dashed black line indicates the approximate path of the trunk stream. The Himalayan crest is indicated by the black dots. Highest erosion rates are predicted along the southern flank of the Himalaya, where catchments straddle the Main Central Thrust (MCT). Regionally, rates are predicted to vary by ~2–2.5 fold. STD, South Tibetan Detachment. (After Brewer *et al.*, 2006.)

conductivity and radioactive heat production on one flank of an orogen are typically thrust over or under rocks on the other flank. In such conditions, isotherms are not just warped by topography, but are strongly perturbed (Fig. 16) by the relatively cold, underthrust slab (Koons, 1989; Harrison *et al.*, 1997; Beaumont *et al.*, 2001; Jamieson *et al.*, 2002). On their way to the orogen's surface in response to erosion, rock particles move obliquely through this thermal field (Stüwe & Hintermüller, 2000; Batt & Brandon, 2002). Although their cooling ages

when they reach the surface still reflect the transport time since crossing the appropriate closure isotherm, their path toward the surface is now oblique and longer than when only the vertical component of motion is considered (Stüwe & Hintermüller, 2000). Hence, lag times now integrate the complete horizontal and vertical travel history of rocks with respect to a warped closure isotherm (Fig. 16).

As a consequence of the above, cooling ages at the surface depend on multiple factors (Ehlers & Farley, 2003; Brewer & Burbank, 2006): the depth of the critical closure isotherm; the particle path from the closure isotherm to the surface; the rate of motion along that particle path toward the surface; and the topographic relief at the surface, which continues to produce differences in ages between valleys and ridges (Fig. 16). If the cooling ages that emerge at the surface can be modelled successfully in this complex thermal and kinematic regime, and if sediment transport times to the basin are short, then detrital cooling ages can be used to gain insight on orogenic dynamics and erosion rates (Brewer & Burbank, 2006).

Although the overall plate convergence rate across an orogen may be known through geodetic or geological data, the way in which that convergence is accommodated is commonly poorly known. For example, with two plates colliding, one of the two could be imagined as passive and unchanging, whereas the other plate would either subduct beneath or override the 'stationary' plate. Although such end-member models rarely apply, the actual amount of convergence that is partitioned into each plate is typically difficult to assess. Nonetheless, that partitioning and associated erosion will define the particle pathways and related thermal histories within an orogen. Here, a model (Brewer & Burbank, 2006) is described that predicts orogenic cooling ages and the resultant detrital ages in a catchment as a function of the partitioning of convergence and erosion rates. Through comparisons of the model predictions with observed detrital ages (Brewer *et al.*, 2006), it is possible to assess various partitioning and erosion scenarios and obtain new insights on orogenic kinematics.

The Himalayan orogen has been examined in this manner, using a simplified numerical model relevant to $^{39}\text{Ar}/^{40}\text{Ar}$ cooling ages of muscovite. At the coarsest scale, the orogen is defined by an underthrusting Indian plate and an overthrusting

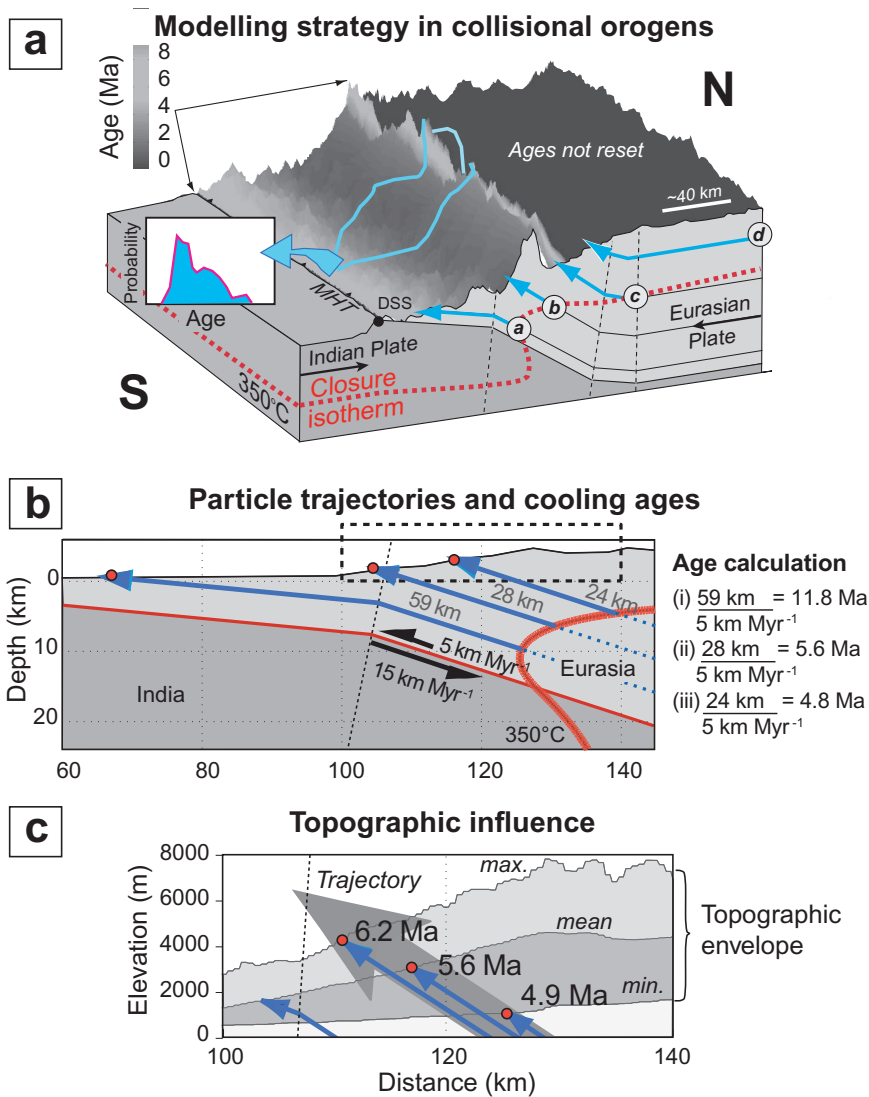


Fig. 16 Conceptual basis for combining thermal and kinematic models to predict a detrital signal in a convergent orogen in which lateral advection rates are high. (a) Given a simplified ramp-flat geometry and known convergence rate, particle velocities and depth to the muscovite closure temperature (350°C) are calculated, assuming thermal and topographic steady state. In a digital elevation model (DEM), an age is calculated for each point based on its position with respect to the closure isotherm and particle pathways to the surface. Ages 'collected' from a catchment in the DEM define the age-population distribution for a detrital sample. Among the particle trajectories (*a-d*), trajectory *b* will have the youngest age because the 350°C isotherm is closest to the surface along this trajectory, while trajectory *d* will have old or un-reset ages. (b) Examples of surface age calculations based on three trajectories and an overthrusting rate of 5 km Myr⁻¹. (c) Particles following the same trajectory in two dimensions commonly travel different distances to the surface due to along-strike changes in topography in a three-dimensional landscape. The predicted effects of maximum, minimum and mean topography on cooling ages are illustrated. (After Brewer & Burbank, 2006.)

Asian plate. (Note that the 'Asian' plate actually consists of accreted Indian plate rocks in the area of interest within the Himalaya.) The overall modelling strategy requires specifying a kinematic geometry that defines how particles move through the thermal structure of the orogen (Fig. 16a). A critical assumption is that the topography is in steady state at the time-scales of interest (10^6 – 10^7 Myr; Willett, 1999): this dictates that the surface erodes at exactly the same rate as rocks are moving along particle pathways toward the surface. Hence, the rate of overthrusting and the rate of erosion are equal, and the rate of cooling is inextricably linked to them, because the thermal structure varies with erosion rate and particle pathway beneath a fixed surface topography. Thermal attributes

in terms of heat production and conductivity are assumed and a two-dimensional kinematic geometry is defined that dictates particle paths. Subsequently, the position of the closure isotherm is solved by assuming a thermal steady state: a condition that requires a few million years to achieve (Brewer *et al.*, 2003). The rate of rock movement along the pathway, the erosion rate and the cooling ages at the surface (Fig. 16b) all depend on how convergence is partitioned into the overriding or underthrusting plate (Brewer & Burbank, 2006).

To extrapolate to a pseudo-three-dimensional model of bedrock cooling ages, it is assumed that the kinematic geometry and thermal characteristics are homogeneous along strike in the orogen, and then the time it takes (i.e. the cooling age) for a particle

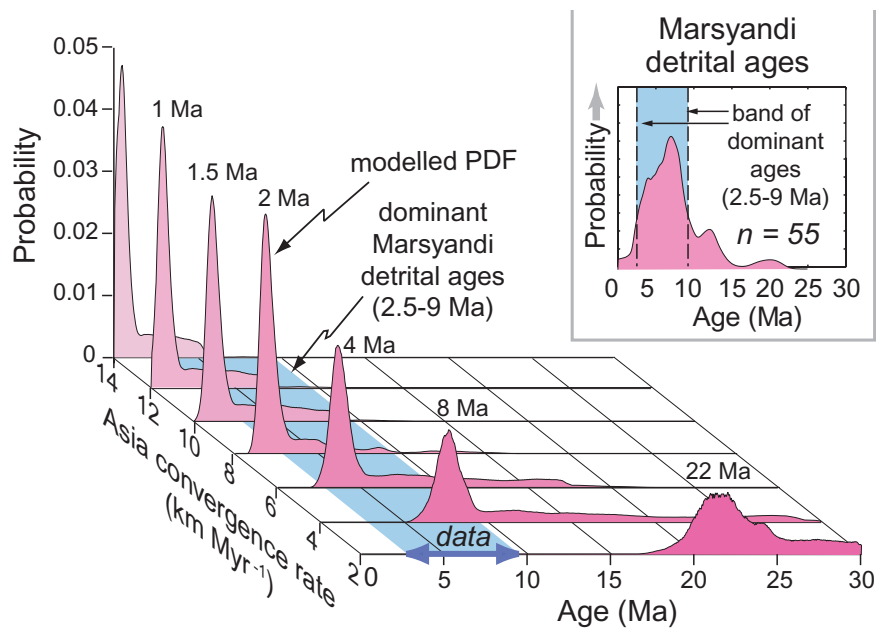


Fig. 17 Modelled detrital cooling-age signals resulting from partitioning the relative convergence rate between India and Asia. Topographic steady state is assumed, such that the erosion and overthrusting rates are equal in the 'Asian' plate. Probability density functions (PDFs) of the predicted age distribution represent the reset age signals from a topographic swath across the Nepalese Himalaya centred on the Marsyandi catchment. The central age for each PDF is shown by the peak in the PDF. The Asian convergence (or overthrusting) rate varies between 2 and 14 km Myr⁻¹, while total convergence rate (20 mm yr⁻¹) and all else remain constant. The inset shows the observed detrital ages from the most downstream site from the Marsyandi River (Brewer *et al.*, 2006) that define the dominant range of ages (blue band) against which the model data are compared. Convergence (or erosion) rates of 4–6 km Myr⁻¹ for Asia provide the best match to the bulk of the observed data. Faster overthrusting (≥ 8 km Myr⁻¹) is predicted to yield ages that are too young, whereas slower overthrusting (≤ 2 km Myr⁻¹) yields ages that are too old. See Fig. 16 for the schematic framework of the age and overthrusting calculations.

to travel from the closure isotherm to the surface along a discrete trajectory to each point on the surface (Fig. 16c) is calculated. These predicted bedrock-cooling ages are then 'extracted' from a catchment in a digital elevation model of the orogen (Fig. 16a) and compared with observed cooling ages from the same catchment. Comparisons of observed ages with those predicted for various scenarios for partitioning overthrusting and underthrusting set clear limits on which scenarios are viable.

This modelling approach, the details of which are described in Brewer & Burbank (2006), has been applied to the Marsyandi catchment in central Nepal. A simple fault-bend fold kinematic model is employed in which the geometry reflects that inferred from deep seismic profiling, modern seismicity and surface geology (Schelling, 1992; Pandey *et al.*, 1995; Nelson *et al.*, 1996; Nábelek *et al.*, 2005). Across the Himalaya, the Indian sub-continent is converging with southern Tibet at a

geodetic rate of ~ 20 mm yr⁻¹ (Bilham *et al.*, 1997; Wang *et al.*, 2001). The goal is to use the observed detrital ages and the numerical model to determine how much of this convergence is partitioned into 'Asian' overthrusting and how much is partitioned into 'Indian' underthrusting.

Given the assumption of topographic steady state, the more convergence that is partitioned into Asian overthrusting, the younger the cooling ages are expected to be within the Himalaya, because erosion rates and overthrusting rates are equivalent (Fig. 17). As extracted from the digital Marsyandi catchment, and based on different overthrusting rates, the predicted cooling ages exhibit dominant age peaks that range from 0.5 Ma to 22 Ma for Asian overthrusting, and erosion rates of 14 mm yr⁻¹ to 2 mm yr⁻¹, respectively (Fig. 17). The observed detrital data from the most downstream sample from the Marsyandi (Figs 14 & 17) are dominated by ages between 4 and 9 Ma. Hence,

both rapid (8–12 mm yr⁻¹) and slow (2 mm yr⁻¹) overthrusting and erosion can be eliminated. The best match to the data clearly occurs for an overthrusting and erosion rate of between 4 and 6 mm yr⁻¹ (Brewer & Burbank, 2006).

Despite many assumptions and simplifications, comparison of the observed detrital age data and model predictions makes it possible to gain useful insights on the Himalayan collision. Previous models that hypothesized overthrusting rates of ~10 mm yr⁻¹ (Harrison *et al.*, 1997) clearly would produce much younger ages than those observed at the surface if the overthrusting rates were analysed within the thermal and kinematic context of the current model. When constrained by detrital ages and assuming a steady-state topography, modelling suggests that only about 25% of the Indo-Tibetan convergence occurs as overthrusting (Fig. 17). Further exploration of orogenic parameters could be accomplished by varying the kinematic geometry or by relaxing some of the model assumptions, such as that regarding steady-state topography. Each such change in the model would yield different cooling ages at the surface. Whereas the temporal resolution afforded by the observed suite of cooling ages is typically limited to a few million years, such precision is sufficient to distinguish among several model predictions.

DISCUSSION

The use of the stratigraphic record to interpret tectonic histories is a core goal of many stratigraphic studies. Advances in geochemical techniques now facilitate analysis of individual minerals. Single-crystal dating of detrital minerals confers a remarkable ability to utilize ages to reconstruct cooling histories of orogens and to place limits on the timing, magnitude and spatial variations of erosion. As opposed to bedrock cooling ages, which are obtained from single outcrops, detrital samples have a tremendous advantage: they comprise minerals drawn from the entire catchment. Thus, detrital samples offer an integrated perspective that is almost always unattainable at the outcrop scale. Moreover, detrital ages are preserved within stratigraphic successions, such that the evolution of cooling ages through time and across an orogen can be reconstructed from the sedimentary

record (e.g. Cervený *et al.*, 1988; Bullen *et al.*, 2001; White *et al.*, 2002).

Despite a burgeoning suite of applications of single-crystal dating to stratigraphic problems, many concepts that underpin interpretations of the data remain poorly explored: the fidelity of the sedimentary detrital age signal with respect to the bedrock ages from which it was derived; the effects of spatial and temporal variations in erosion on detrital ages; the ability of detrital ages to record subtle variations in erosion; the influence of variable source-area lithology and grain sizes on detrital ages. In this study, an attempt has been made to quantify several key controls on detrital ages and to examine some new applications of detrital ages to tectonic interpretations.

When a research objective is to define the initiation of major deformation, low-temperature dating approaches, such as apatite fission track or [U-Th]/He (Stockli *et al.*, 2000; Ehlers & Farley, 2003), are typically preferable because the shallow depth of the closure isotherm renders it particularly sensitive to surface cooling due to erosion. Not only do these dating approaches utilize a low-temperature thermochronometer that varies spatially at shallow depths due to warping of the closure isotherm beneath topographic relief (Stüwe *et al.*, 1994), but the existence of a partial annealing zone for fission-track dating and a partial retention zone for [U-Th]/He dating (Wolf *et al.*, 1996) generates distinctive changes in cooling ages within this thermal layer. Low-temperature dating of detrital grains is particularly well suited for dating of nascent uplifts and for slowly eroding ranges (Naeser *et al.*, 1983; Sobel & Dumitru, 1997; Blythe, 2002). In rapidly eroding ranges (≥ 2 –4 mm yr⁻¹), the paucity in fission tracks in most apatite crystals increases analytical uncertainties and limits the age resolution. For example, along the Marsyandi River within the Greater Himalaya, apatite fission-track bedrock cooling ages are very young (~0.5 Ma) and have large uncertainties (20–50%; Burbank *et al.*, 2003) that preclude detailed analyses of detrital apatite grains. Dating of apatite by [U-Th]/He utilizes an even lower closure temperature (~70°C) and presents similar analytical challenges in rapidly eroded sediments.

The closure isotherm (~350°C) for ³⁹Ar/⁴⁰Ar dates on muscovite remains nearly insensitive to topography, as long as erosion rates and topographic

relief are less than 3 mm yr^{-1} and 6 km, respectively (Fig. 3). As a consequence, cooling-age variations are easy to predict as a function of altitude. On the other hand, interpretations of cooling ages as recorders of erosion rates are complicated by typical detrital muscovite ages that range into millions of years (Carrapa *et al.*, 2003, 2004). Changes in erosion rates, thermal regimes and kinematic pathways are likely to occur during the extended time it takes a rock to transit from the closure isotherm to the surface, and it commonly requires several million years to attain a new thermal equilibrium (Brewer *et al.*, 2003).

Studies from the Kyrgyz Range in the Tien Shan suggest that detrital fission-track ages can provide a faithful sampling of the distribution of cooling ages within a given catchment. When erosion rates are relatively slow ($0.1\text{--}1 \text{ mm yr}^{-1}$), as seen in the Kyrgyz Range, and the kinematic geometry is simple (Fig. 12d), detrital ages can be sensitive to differences of as little as 1–2 km in the magnitude of erosion. Slow erosion rates underpin this sensitivity, because they allow incremental incision through a stratigraphy of bedrock cooling ages (Stock & Montgomery, 1996), thereby producing discernible variations in the detrital ages derived from an eroding range. Under such circumstances, spatial differences in detrital ages along a range can record differential incision (Bullen *et al.*, 2001). It is important to note that these Kyrgyz examples are drawn from simple catchments draining a single range, such that variations in detrital ages can be linked directly to erosion in the nearby mountains. In typical foreland basins, however, multiple sources feed sediment into the basin, and the detrital age signal is expected to be a complex integration of those sources. To minimize the uncertainty in source areas in pre-Quaternary orogens, samples should be drawn from sections where provenance studies suggest a consistent source area and palaeocurrent directions indicate transverse flow. Rivers with this orientation are more likely to drain a simple orogenic catchment, whereas longitudinal rivers almost always drain a broad suite of hinterland catchments (Burbank, 1992).

Analyses in active orogens of detrital ages in modern rivers, such as the Marsyandi River in the Nepalese Himalaya (Fig. 14), clearly demonstrate a striking downstream evolution of the suite of ages. This evolution results from convolving the sediment

fluxes from each tributary catchment, each of those fluxes being dependent on catchment size, erosion rate and abundance of the mineral targeted for dating. Two important aspects that are related to the interpretation of detrital ages in stratigraphic successions emerge from the analysis of the modern Marsyandi sediment. First, major parts of a given catchment may be poorly represented in the detrital signal preserved in a sedimentary basin. Immediately upstream of the junction of the Marsyandi and Trisuli Rivers, for example, almost no detrital ages from the northern 50% of the catchment are represented among the 56 grains dated. Rapid erosion within more downstream tributaries apparently overwhelms the contributions from upstream. Second, spatial variations in the abundance of the mineral targeted for dating can exert a major control on the detrital age signal that emerges from a range. In the Marsyandi catchment, a >100-fold variation is observed in muscovite abundances among catchment areas varying from 10^2 to 10^3 km^2 . Zircon, another mineral commonly used for detrital single-crystal dating, has up to eightfold differences in abundance in the Greater and Lesser Himalaya, and is almost absent from a few regions (Amidon *et al.*, 2005a). Quantitative analyses of detrital ages that assume uniform mineral distribution can be biased by ignoring the actual variability in mineral abundance. Although abundances of commonly occurring minerals such as muscovite can be determined through point counting, determining the grain frequency of zircon or apatite, which occur in trace amounts, is more tedious. Amidon *et al.* (2005b) have recently developed a methodology based on grain shape and volume that generates an estimate of zircon abundance within the size fraction being dated with a precision of $\pm 10\%$: a resolution better than that typically achieved with point counting of sparse minerals (Van der Plas & Tobi, 1965; Brewer *et al.*, 2006).

In analyses such as the attempt to calculate erosion rates within the Marsyandi (Fig. 15), a trade-off exists between spatial resolution and research investment. Clearly, by dividing the Marsyandi catchment into tributary catchments, a more highly resolved image of spatial variations in erosion rates is attainable than if the entire catchment were modelled as a uniformly eroding entity. The tributary catchments themselves, however, are typically

> 200 km² and would be expected to have variations in erosion rates within them. Further subdivision of each catchment, additional detrital mineral dates and measurement of variations in muscovite abundance (the target mineral for dating) would be required to refine the erosion-rate estimates.

In collisional orogens, the lateral component of particle pathways should not be ignored, because ages observed at the surface depend on the oblique trajectories of rocks through the orogen. In addition to the altitudinal dependence of ages that pertains when rocks move only vertically toward the surface, a spatial dependence will exist that reflects the intersection of the closure isotherm with various particle trajectories. Thus, even with uniform erosion across an orogen, cooling ages may differ by several fold when rocks from proximal and distal sites are compared. If an appropriate kinematic and thermal model can be developed, detrital ages derived from the orogen can be used to test large-scale kinematic parameters, such as average rates of overthrusting.

As single-crystal dating of detrital minerals becomes more efficient and less expensive, many of the assumptions that underpin current interpretations can be more systematically tested. In addition, it will be possible to quantify modern fluvial systems much more thoroughly, in order to understand how detrital ages evolve within a variably eroding and lithological heterogeneous mountain range. Finally, combining observed detrital ages with improved numerical models should permit further exploration of the dynamics of orogens and the diversity of erosion styles and rates.

CONCLUSIONS

Whereas many methodological improvements can be envisioned to render analyses of detrital ages more robust, the advent of single-crystal dating has opened a new era in the analysis of both stratigraphic successions and geomorphic systems. Studies of modern systems demonstrate how the detrital signal is generated, and reveal both the power and limitations of single-crystal dating in sedimentary basins. Although recognized previously from a theoretical viewpoint, the impact exerted on modern detrital ages by the interplay between erosion rates and lithology within numerous tributaries has only recently been documented,

and provides a basis for refining orogenic histories using detrital ages. These studies of modern rivers provide both insights and cautions with respect to the interpretation of detrital ages within the stratigraphic record: detrital ages can record subtle variations in the history of erosion and rock uplift, but rapidly eroding areas can overwhelm slowly eroding ones and lithological variability can introduce strong biases in detrital ages. An ability to exploit detrital ages to constrain kinematic rates within collisional orogens provides a potent new analytical tool. If uncertainties regarding kinematic geometries and related particle pathways through orogens can be reduced, detrital ages in both modern rivers and the recent stratigraphic record can serve to reconstruct rates of deformation and erosion and to test the viability of proposed models of orogenic evolution.

ACKNOWLEDGEMENTS

This research was primarily supported by grants from the National Science Foundation (EAR-9627865, 9614765, 9909647) and NASA (NAG5-9039; 10520; 13758). We are grateful for helpful discussions with M. Brandon, W. Amidon and R. Slingerland, and for the contributions of Mike Oskin and Bodo Bookhagen with respect to the digital elevation model analysis. We thank John Garver for his assistance with the fission-track analyses. Incisive reviews by C. Paola and T. Ehlers greatly improved this manuscript.

REFERENCES

- Amidon, W.H., Burbank, D.W. and Gehrels, G.E. (2005a) Construction of foreland mineral populations: insights from mixing of U–Pb zircon ages in Himalayan rivers. *Basin Res.*, **17**, 463–485.
- Amidon, W.H., Burbank, D.W. and Gehrels, G.E. (2005b) U–Pb zircon ages as a sediment mixing tracer in the Nepal Himalaya. *Earth Planet. Sci. Lett.*, **235**, 244–260.
- Batt, G.E. and Brandon, M.T. (2002) Lateral thinking: 2-D interpretation of thermochronology in convergent orogenic settings. *Tectonophysics*, **349**, 185–201.
- Beaumont, C., Jamieson, R.A., Nguyen, M.H. and Lee, B. (2001) Himalayan tectonics explained by extrusion of a low-viscosity crustal channel coupled to focused surface denudation. *Nature*, **414**, 738–742.

- Bernet, M., Brandon, M.T., Garver, J.I. and Molitor, B.R. (2004a) Downstream changes of Alpine zircon fission-track ages in the Rhône and Rhine Rivers. *J. Sediment. Res.*, **74**, 82–94.
- Bernet, M., Brandon, M.T., Garver, J.I. and Molitor, B.R. (2004b) Fundamentals of detrital zircon fission-track analysis for provenance and exhumation studies with examples from the European Alps. In: *Detrital Thermochronology—Provenance Analysis, Exhumation, and Landscape Evolution of Mountain Belts* (Eds M. Bernet and C. Spiegel). *Geol. Soc. Am. Spec. Pap.*, **378**, 25–36.
- Billham, R., Larson, K. and Freymueller, J. (1997) GPS measurements of the present-day convergence across the Nepal Himalaya. *Nature*, **386**, 61–63.
- Blythe, A.E., House, M.A. and Spotila, J. (2002) Low-temperature thermochronology of the San Gabriel and San Bernardino Mountains, southern California: constraining structural evolution. In: *Contributions to Crustal Evolution of the Southwestern United States* (Ed. A.P. Barth). *Geol. Soc. Am. Spec. Pap.*, **365**, 231–250.
- Bollinger, L., Avouac, J.P., Beyssac, O., *et al.* (2004) Thermal structure and exhumation history of the Lesser Himalaya in central Nepal. *Tectonics*, **23**, TC5015, doi:10.1029/2003TC001564.
- Brandon, M.T. (1992) Decomposition of fission-track grain-age distributions. *Am. J. Sci.*, **292**, 535–564.
- Brandon, M.T. (1996) Probability density plot for fission-track grain-age samples. *Radiat. Meas.*, **26**, 663–676.
- Brandon, M.T. (2002) Decomposition of mixed grain-age distributions using BINOMFIT. *On Track*, **24**, 13–18.
- Brandon, M.T. and Vance, J.A. (1992) Fission-track ages of detrital zircon grains: implications for the tectonic evolution of the Cenozoic Olympic subduction complex. *Am. J. Sci.*, **292**, 565–636.
- Brewer, I.D. (2001) *Detrital-mineral thermochronology: investigations of orogenic denudation in the Himalaya of central Nepal*. Unpublished PhD thesis, Pennsylvania State University, 201 pp.
- Brewer, I.D., Burbank, D.W. and Hodges, K.V. (2003) Modelling detrital cooling-age populations: insights from two Himalayan catchments. *Basin Res.*, **15**, 305–320.
- Brewer, I.A., Burbank, D.W. and Hodges, K.V. (2006) Downstream development of a detrital cooling-age signal: Insights from $^{40}\text{Ar}/^{39}\text{Ar}$ muscovite thermochronology in the Nepalese Himalaya. *Geol. Soc. Am. Spec. Pap.*, **398**, 321–338.
- Brewer, I.D. and Burbank, D.W. (2006) Thermal and kinematic modeling of bedrock and detrital cooling ages in the Central Himalaya. *J. Geophys. Res.*, **III**, B09409, doi: 09410.01029/02004JB0003304.
- Brown, R.W. (1991) Backstacking apatite fission-track 'stratigraphy': a method for resolving the erosional and isostatic components of tectonic uplift histories. *Geology*, **19**, 74–77.
- Bullen, M.E., Burbank, D.W., Abdrakhmatov, K.Y. and Garver, J. (2001) Late Cenozoic tectonic evolution of the northwestern Tien Shan: constraints from magnetostratigraphy, detrital fission track, and basin analysis. *Geol. Soc. Am. Bull.*, **113**, 1544–1559.
- Bullen, M.E., Burbank, D.W. and Garver, J.I. (2003) Building the northern Tien Shan: integrated thermal, structural, and topographic constraints. *J. Geol.*, **111**, 149–165.
- Burbank, D.W. (1992) Causes of recent Himalayan uplift deduced from deposited patterns in the Ganges basin. *Nature*, **357**, 680–682.
- Burbank, D.W., Blythe, A.E., Putkonen, J., *et al.* (2003) Decoupling of erosion and precipitation in the Himalayas. *Nature*, **426**, 652–655.
- Carrapa, B., Wijbrans, J. and Bertotti, G. (2003) Episodic exhumation in the Western Alps. *Geology*, **31**, 601–604.
- Carrapa, B., Wijbrans, J. and Bertotti, G. (2004) Detecting provenance variations and cooling patterns within the western Alpine orogen through $^{40}\text{Ar}/^{39}\text{Ar}$ geochronology on detrital sediments: The Tertiary Piedmont Basin, northwest Italy. In: *Detrital Thermochronology—Provenance Analysis, Exhumation, and Landscape Evolution of Mountain Belts* (Eds M. Bernet and C. Spiegel). *Geol. Soc. Am. Spec. Pap.*, **378**, 67–103.
- Carter, A. (1999) Present status and future avenues of source region discrimination and characterization using fission track analysis. *Sediment. Geol.*, **124**, 31–45.
- Carter, A. and Moss, S.J. (1999) Combined detrital-zircon fission-track and U–Pb dating: a new approach to understanding hinterland evolution. *Geology*, **27**, 235–238.
- Cervený, P.F., Naeser, N.D., Zeitler, P.K., Naeser, C.W. and Johnson, N.M. (1988) History of uplift and relief of the Himalaya during the past 18 million years; evidence from sandstones of the Siwalik Group. In: *New Perspectives in Basin Analysis* (Eds K.L. Kleinspehn and C. Paola), pp. 43–61. Springer-Verlag, New York.
- Davis, G.A. (1988) Rapid upward transport of mid-crustal mylonitic gneisses in the footwall of a Miocene detachment fault, Whipple Mountains, southeastern California. *Int. J. Earth Sci.*, **77**, 191–209.
- Dodson, M.H. (1979) Theory of cooling ages. In: *Lectures in Isotope Geology* (Eds E. Jaeger and C.J. Hunziker), pp. 194–202. Springer-Verlag, New York.
- Ehlers, T.A. and Farley, K.A. (2003) Apatite (U–Th)/He thermochronometry: methods and applications to problems in tectonic and surface processes. *Earth Planet. Sci. Lett.*, **206**, 1–14.
- Ehlers, T.A., Willett, S.D., Armstrong, P.A. and Chapman, D.S. (2003) Exhumation of the central

- Wasatch Mountains, Utah: 2. Thermokinematic model of exhumation, erosion, and thermochronometer interpretation. *J. Geophys. Res.*, **108**, 2173, doi:10.1029/2001JB001723.
- Farley, K.A. (2000) Helium diffusion from apatite; general behavior as illustrated by Durango fluorapatite. *J. Geophys. Res.*, **105**, 2903–2914.
- Fitzgerald, P.G., Sorkhabi, R.B., Redfield, T.F. and Stump, E. (1995) Uplift and denudation of the central Alaska Range: a case study in the use of apatite fission track thermochronology to determine absolute uplift parameters. *J. Geophys. Res.*, **100**, 20,175–20,191.
- Gallagher, K., Brown, R. and Johnson, C. (1998) Fission track analysis and its applications to geological problems. *Ann. Rev. Earth Planet. Sci.*, **26**, 519–572.
- Garver, J.I. and Brandon, M.T. (1994) Erosional exhumation of the British Columbia Coast Ranges as determined from fission-track ages of detrital zircon from the Tofino basin, Olympic Peninsula, Washington. *Geol. Soc. Amer. Bull.*, **106**, 1398–1412.
- Garver, J.I., Brandon, M.T., Roden-Tice, M. and Kamp, P.J.J. (1999) Exhumation history of orogenic highlands determined by detrital fission-track thermochronology. In: *Exhumation Processes; Normal Faulting, Ductile Flow and Erosion* (Eds U. Ring, M.T. Brandon, G.S. Lister and S. Willett), pp. 283–304. Special Publication 154, Geological Society Publishing House, Bath.
- Gehrels, G.E. and Kapp, P.A. (1998) Detrital zircon geochronology and regional correlation of metasedimentary rocks in the Coast Mountains, southeastern Alaska. *Can. J. Earth Sci.*, **35**, 269–279.
- Green, P.F., Duddy, I.R., Gleadow, A.J.W. and Lovering, J.F. (1989) Apatite fission track analysis as a paleotemperature indicator for hydrocarbon exploration. In: *Thermal History of Sedimentary Basins: Methods and Case Histories* (Eds N.D. Naeser and T.H. McCulloh), pp. 181–195. Springer-Verlag, New York.
- Harrison, T.M., Ryerson, F.J., Le Fort, P., Yin, A., Lovera, O.M. and Catlos, E.J. (1997) A late Miocene–Pliocene origin for the central Himalayan inverted metamorphism. *Earth Planet. Sci. Lett.*, **146**, E1–E7.
- Harrison, T.M., Grove, M., Lovera, O.M. and Catlos, E.J. (1998) A model for the origin of Himalayan anatexis and inverted metamorphism. *J. Geophys. Res.*, **103**, 27,017–27,032.
- Hasbargen, L. and Paola, C. (2000) Landscape instability in an experimental drainage basin. *Geology*, **28**, 1067–1070.
- Hasbargen, L. and Paola, C. (2002) How predictable is local erosion rate in erosional landscapes? In: *Prediction in Geomorphology* (Eds P.R. Wilcock and R.M. Iverson), pp. 231–240. Monograph 135, American Geophysical Union, Washington, DC.
- Hodges, K.V. (2000) Tectonics of the Himalaya and southern Tibet from two perspectives. *Geol. Soc. Am. Bull.*, **112**, 324–350.
- Hodges, K., Wobus, C., Ruhl, K., Schildgen, T. and Whipple, K. (2004) Quaternary deformation, river steepening, and heavy precipitation at the front of the Higher Himalayan ranges. *Earth Planet. Sci. Lett.*, **220**, 379–389.
- Jamieson, R.A., Beaumont, C., Nguyen, M.H. and Lee, B. (2002) Interaction of metamorphism, deformation and exhumation in large convergent orogens. *J. Metamorph. Geol.*, **20**, 9–24.
- Jamieson, R.A., Beaumont, C., Medvedev, S. and Nguyen, M.H. (2004) Crustal channel flows: 2. Numerical models with implications for metamorphism in the Himalayan-Tibetan orogen. *J. Geophys. Res.*, **109**, B06407, doi:10.1029/2003JB002811.
- Johnson, N.M., Stix, J., Tauxe, L., Cervený, P.F. and Tahirkheli, R.A.K. (1985) Paleomagnetic chronology, fluvial processes, and tectonic implications of the Siwalik deposits near Chinji Village, Pakistan. *J. Geol.*, **93**, 27–40.
- Ketchum, R.A., Donelick, R.A. and Carlson, W.D. (1999) Variability of apatite fission-track annealing kinetics: III. Extrapolation to geologic time scales. *Amer. Mineral.*, **84**, 1235–1255.
- Koons, P.O. (1989) The topographic evolution of collisional mountain belts: a numerical look at the Southern Alps, New Zealand. *Am. J. Sci.*, **289**, 1041–1069.
- Mancktelow, N.S. and Grasemann, B. (1997) Time-dependent effects of heat advection and topography on cooling histories during erosion. *Tectonophysics*, **270**, 167–195.
- McDougall, I. and Harrison, T.M. (1988) *Geochronology and Thermochronology by the $^{40}\text{Ar}/^{39}\text{Ar}$ Method*. Oxford University Press, New York, 212 pp.
- Nábelek, J.L., Vergne, J., Hetenyi, G. and Team, H.-C. (2005) Project Hi-CLIMB: a synoptic view of the Himalayan collision zone and Southern Tibet. *Eos Trans. AGU Fall Meet. Suppl.*, **86**, T52A-02.
- Naeser, C.W. (1979) Fission-track dating and geological annealing of fission tracks. In: *Lectures in Isotope Geology* (Eds E. Jäger and J.C. Hunziker), pp. 154–169. Springer-Verlag, New York.
- Naeser, C.W., Bryant, B., Crittenden, M.D., Jr. and Sorensen, M.L. (1983) Fission-track ages of apatite in the Wasatch Mountains, Utah: an uplift study. *Geol. Soc. Am. Mem.*, **157**, 29–36.
- Najman, Y., Pringle, M., Godin, L. and Oliver, G. (2001) Dating of the oldest continental sediments from the Himalayan foreland basin. *Nature*, **410**, 194–197.
- Nelson, K.D., Zhao, W., Brown, L.D., et al. (1996) Partially molten middle crust beneath southern Tibet;

- synthesis of Project INDEPTH result. *Science*, **274**, 1684–1688.
- Pandey, M.R., Tandukar, R.P., Avouac, J.P., Lavé, J. and Massot, J.P. (1995) Interseismic strain accumulation on the Himalayan crustal ramp (Nepal). *Geophys. Res. Lett.*, **22**, 751–754.
- Pelletier, J.D. (2004) Persistent drainage migration in a numerical landform evolution model. *Geophys. Res. Lett.*, **31**, doi:10.1029/2004GL020802.
- Reiners, P.W., Spell, T.L., Nicolescu, S. and Zanetti, K.A. (2004) Zircon (U–Th)/He thermochronometry: He diffusion and comparisons with $^{40}\text{Ar}/^{39}\text{Ar}$ dating. *Geochim. Cosmochim. Acta*, **68**, 1857–1887.
- Ruhl, K.W. and Hodges, K.V. (2005) The use of detrital mineral cooling ages to evaluate steady-state assumptions in active orogens: an example from the central Nepalese Himalaya. *Tectonics*, **24**, TC4015, 10.1029/2004TC001712.
- Ruiz, G.M.H., Seward, D. and Winkler, W. (2004) Detrital thermochronology – a new perspective on hinterland tectonics, an example from the Andean Amazon Basin, Ecuador. *Basin Res.*, **16**, 413–430.
- Schelling, D. (1992) The tectonostratigraphy and structure of the eastern Nepal Himalaya. *Tectonics*, **11**, 925–943.
- Small, E.E. and Anderson, R.A. (1998) Pleistocene relief production in Laramide mountain ranges, western United States. *Geology*, **26**, 123–136.
- Sobel, E.R. and Dumitru, T.A. (1997) Thrusting and exhumation around the margins of the western Tarim basin during the Indian-Asia collision. *J. Geophys. Res.*, **102**, 5043–5063.
- Sobel, E.R., Oskin, M., Burbank, D. and Mikolaichuk, A. (2006) Exhumation of basement-cored uplifts: Example of the Kyrgyz Range quantified with apatite fission-track thermochronology. *Tectonics*, **25**, TC2008, 10.1029/2005TC001809.
- Spiegel, C., Siebel, W., Kuhlemann, J. and Frisch, W. (2004) Toward a comprehensive provenance analysis: a multi-method approach and its implications for the evolution of the Central Alps. In: *Detrital Thermochronology – Provenance Analysis, Exhumation, and Landscape Evolution of Mountain Belts* (Ed. M. Bernet and C. Spiegel). *Geol. Soc. Am. Spec. Pap.* **378**, 37–50.
- Stock, J.D. and Montgomery, D.R. (1996) Estimating palaeorelief from detrital mineral age ranges. *Basin Res.*, **8**, 317–328.
- Stockli, D., Farley, K.A. and Dumitru, T.A. (2000) Calibration of the apatite (U–Th)/He thermochronometer on an exhumed fault block, White Mountains, California. *Geology*, **28**, 983–986.
- Stüwe, K. and Hintermüller, M. (2000) Topography and isotherms revisited: The influence of laterally migrating drainage divides. *Earth Planet. Sci. Lett.*, **184**, 287–303.
- Stüwe, K., White, L. and Brown, R. (1994) The influence of eroding topography on steady-state isotherms: application to fission track analysis. *Earth Planet. Sci. Lett.*, **124**, 63–74.
- Tippett, J.M. and Kamp, P.J.J. (1993) Fission track analysis of the Late Cenozoic vertical kinematics of continental Pacific crust, South Island, New Zealand. *J. Geophys. Res.*, **98**, 16,119–16,148.
- Van der Plas, L. and Tobi, A.C. (1965) A chart for judging the reliability of point counting results. *Am. J. Sci.*, **263**, 87–90.
- Vermeesch, P. (2004) How many grains are needed for a provenance study? *Earth Planet. Sci. Lett.*, **224**, 441–451.
- Wang, Q., Zhang, P.-Z., Freymueller, J.T., *et al.* (2001) Present-day crustal deformation in China constrained by Global Positioning System measurements. *Science*, **294**, 574–577.
- White, N.M., Pringle, M., Garzanti, E., *et al.* (2002) Constraints on the exhumation and erosion of the High Himalayan Slab, NW India, from foreland basin deposits. *Earth Planet. Sci. Lett.*, **195**, 29–44.
- Willett, S.D. (1999) Orogeny and orography: the effects of erosion on the structure of mountain belts. *J. Geophys. Res.*, **104**, 28,957–28,982.
- Willett, S.D. and Brandon, M.T. (2002) On steady states in mountain belts. *Geology*, **30**, 175–178.
- Wobus, C.W., Hodges, K.V. and Whipple, K.X. (2003) Has focused denudation sustained active thrusting at the Himalayan topographic front? *Geology*, **31**, 861–864.
- Wolf, R.A., Farley, K.A. and Silver, L.T. (1996) Helium diffusion and low temperature thermochronometry of apatite. *Geochim. Cosmochim. Acta*, **60**, 4231–4240.
- Yamada, R., Tagami, T., Nishimura, S. and Ito, H. (1995) Annealing kinetics of fission tracks in zircon: an experimental study. *Chem. Geol.*, **122**, 249–258.
- Zeitler, P.K. (1985) Cooling history of the NW Himalaya, Pakistan. *Tectonics*, **4**, 127–151.
- Zhang, P., Molnar, P. and Downs, W.R. (2001) Increased sedimentation rates and grain sizes 2–4 Myr ago due to the influence of climate change on erosion rates. *Nature*, **410**, 891–897.

